

Thesis for the degree of Doctor of Philosophy

# Catalytic formation of ammonia from nitric oxide

Emma Catherine Adams



**CHALMERS**

Department of Chemistry and Chemical Engineering

CHALMERS UNIVERSITY OF TECHNOLOGY

Gothenburg, Sweden 2016

Catalytic formation of ammonia from nitric oxide  
Emma Catherine Adams

© Emma Catherine Adams, 2016.

ISBN: 978-91-7597-477-4

Doktorsavhandlingar vid Chalmers tekniska högskola  
Ny serie Nr. 4158  
ISSN: 0346-718X

Department of Chemistry and Chemical Engineering  
Chalmers University of Technology  
SE-412 96 Gothenburg Sweden  
Telephone: +46 (0)31 772 1000

Printed by:  
Chalmers Reproservice  
Gothenburg, Sweden (2016)

## Catalytic formation of ammonia from nitric oxide

Emma Catherine Adams

Department of Chemistry and Chemical Engineering

Chalmers University of Technology, Gothenburg 2016

### Abstract

The emission of nitrogen oxides ( $\text{NO}_x$ ) from automobiles results in severe environmental and biological effects. Passive selective catalytic reduction (passive SCR) of  $\text{NO}_x$  with ammonia ( $\text{NH}_3$ ) is a proposed method for abatement of  $\text{NO}_x$  emissions in net lean-burn gasoline passenger vehicles. The principle idea of this technique is to selectively reduce  $\text{NO}_x$  to nitrogen and water in the presence of excess oxygen by utilising a supply of  $\text{NH}_3$  that has been formed onboard the vehicle over an ammonia formation catalyst (AFC). The aim of this thesis work is to deepen the understanding of how ammonia can be formed from nitric oxide over noble metal based catalysts.

A bottom-up methodology has been employed where model catalysts with increasing complexity have been synthesised and characterised with several methods (BET, ICP-OES, XRD and TEM). The catalytic activity and selectivity for  $\text{NH}_3$  formation have been studied using steady-state and transient experiments in chemical flow-reactors. Also, a number of *in situ* and *operando* experimental techniques, including infrared and X-ray absorption spectroscopy, have been used to reveal catalyst structure-function relationships.

This thesis shows that Pd/Ce/ $\text{Al}_2\text{O}_3$  is a promising base for AFC formulations. This AFC exhibits high activity for  $\text{NH}_3$  formation in the presence of model feed gas mixtures using either a direct source of hydrogen or hydrogen formed *via* the water-gas-shift reaction. It also has higher  $\text{NH}_3$  formation activity than a three-way catalyst when using complex feed compositions containing reactants relevant to those one may encounter onboard lean-burn gasoline vehicles.

The suppression of ammonia formation in net-oxidizing feeds is also investigated. In addition to oxidation of the reductant, a rapid growth in metal-oxides occurs as the feed becomes net-oxidizing. When oxidized, weak interaction between the noble metal phase and NO occurs, resulting in negligible NO dissociation. As dissociative adsorption of NO is a prerequisite step for  $\text{NH}_3$  formation, this is identified as the limiting step for  $\text{NH}_3$  formation from NO and  $\text{H}_2$  in net-oxidizing conditions.

Further, low-temperature ammonia formation is proposed as an important future area of research and the expansion towards utilisation of renewable fuels (alcohols) may open for even more efficient  $\text{NH}_3$  formation over suitable catalysts.

**Keywords:** Environmental heterogeneous catalysis; Passive-SCR; Ammonia formation;  $\text{NO}_x$  reduction; *In situ* characterisation;



## List of Publications

This thesis is based on the work contained in the following publications, referred to by Roman numerals (I-VII) in the text:

- I. Passive SCR: The effect of H<sub>2</sub> to NO ratio on the formation of NH<sub>3</sub> over alumina supported platinum and palladium catalysts**  
Emma Catherine Adams\*, Magnus Skoglundh, Pär Gabrielsson and Per-Anders Carlsson  
*Topics in Catalysis* **59** (2016) 970-975.
- II. Ammonia formation over supported platinum and palladium catalysts**  
Emma Catherine Adams\*, Magnus Skoglundh, Milica Folic, Eva Charlotte Bendixen, Pär Gabrielsson and Per-Anders Carlsson  
*Applied Catalysis B: Environmental* **165** (2015) 10-19.
- III. Ammonia formation over Pd/Al<sub>2</sub>O<sub>3</sub> modified with cerium and barium**  
Emma Catherine Adams\*, Magnus Skoglundh, Pär Gabrielsson, Mats Laurell and Per-Anders Carlsson  
*Catalysis Today* **267** (2016) 210-216.
- IV. Water-gas-shift assisted ammonia formation over Pd/Ce/Alumina**  
Emma Catherine Adams\*, Magnus Skoglundh, Tobias Elmøe and Per-Anders Carlsson  
*Submitted manuscript*
- V. Ammonia formation from nitrogen oxide over Pd-based catalysts in complex feed gas compositions**  
Emma Catherine Adams\*, Magnus Skoglundh, and Per-Anders Carlsson  
*Submitted manuscript*
- VI. Structure function relationship for alumina supported platinum during formation of ammonia from nitrogen oxide and hydrogen in presence of oxygen**  
Emma Catherine Adams\*, Lindsay Richard Merte, Anders Hellman, Magnus Skoglundh, Johan Gustafson, Eva Charlotte Bendixen, Pär Gabrielsson, Florian Bertram, Jonas Evertsson, Chu Zhang, Stefan Carlson and Per-Anders Carlsson  
*Physical Chemistry Chemical Physics* **18** (2016) 10850-10855.
- VII. Operando spectroscopic study of ammonia formation over Pd/Ce/Alumina**  
Emma Catherine Adams\*, Anders Hellman, Magnus Skoglundh, Johan Nilsson, Natalia Martin, Giovanni Agostini, Olivier Mathon and Per-Anders Carlsson  
*Manuscript in progress*

Additional publications, not included in this thesis:

**Effect of thermal ageing on the nature of iron species in Fe-BEA**

S Shwan\*, E C Adams, J Jansson, M Skoglundh

*Catalysis Letters* **143** (2013) 43-48.

**Comparison of lab versus engine tests in the development of a highly efficient ammonia formation catalyst for a passive SCR system**

G Doornbos\*, E C Adams, P-A Carlsson, D Dahl, M Laurell, H Schyllander, P Gabrielsson, M Folic, I Denbratt and M Skoglundh

*SAE Technical Papers* (2015) doi:10.4271/2015-24-2504.

**Spatially and temporally resolved gas distributions around heterogeneous catalysts using infrared planar laser-induced fluorescence**

J Zetterberg\*, S Blomberg, J Gustafson, J Evertsson, J Zhou, E C Adams, P-A Carlsson, M Aldén and E Lundgren

*Nature Communications* **6** (2015) 7076.

**Characterization of surface structure and oxidation/reduction behaviour of Pd-Pt/Al<sub>2</sub>O<sub>3</sub> model catalysts**

N M Martin\*, J Nilsson, M Skoglundh, E C Adams, X Wang, P Velin, G Smedler, A Raj, D Thompsett, H H Brongersma, T Grehl, G Agostini, O Mathon, S Carlson, K Noren, F J Martinez-Casado, Z Matej, O Balmes and P-A Carlsson

*Submitted to Journal of Physical Chemistry C*

**Methane oxidation over Pd/Al<sub>2</sub>O<sub>3</sub> under lean cycling followed by in situ XAFS and modulation excitation spectroscopy**

J Nilsson\*, P-A Carlsson, N M Martin, E Adams, G Agostini, H Grönbeck and M Skoglundh

*Submitted to ACS Catalysis*

**Study of methane oxidation over Pd-Pt catalysts using in situ DRIFTS and XAS techniques**

N M Martin\*, J Nilsson, M Skoglundh, E C Adams, X Wang, G Smedler, A Raj, D Thompsett, G Agostini, S Carlson, K Norén and P-A Carlsson

*Submitted to Catalysis, Structure and Reactivity*

## My contributions to the papers

### **Paper I**

For this paper I prepared the samples and conducted all experiments. I then interpreted the results with my co-authors and was responsible for writing the first draft and submission of the manuscript.

### **Paper II**

I prepared all samples, conducted XRD and surface-area analysis of the samples and performed all flow-reactor and IR experiments. Together with my co-authors I then interpreted these experiments and was responsible for writing the first draft and submission of the manuscript.

### **Paper III**

I was responsible for the preparation and surface-area determination of the samples. I conducted all experiments, interpreted the results together with my co-authors, and was responsible for the writing the first draft and submission of the manuscript.

### **Paper IV**

For this paper I prepared and characterised the specific surface area, oxygen storage capacity and Pd dispersion of all samples. I performed all experiments and, together with my co-authors, interpreted the results and was responsible for writing the first draft and submission of the manuscript.

### **Paper V**

I contributed by preparation of the Pd/Ce/Al<sub>2</sub>O<sub>3</sub> sample. I performed all experiments and determined the oxygen storage capacity of each washcoated monolith. I then, together with my co-authors, interpreted the results and was responsible for writing the first draft and submission of the manuscript.

### **Paper VI**

I contributed by preparing the sample, conducting and interpreting the IR experiments. I performed the XAS experiments at the MAX IV Laboratory together with my co-authors and was responsible for writing the first draft and submission of the manuscript.

### **Paper VII**

I contributed by preparing the sample and conducting the IR experiments. I performed the XAS experiments at ESRF together with my co-authors and was responsible for writing the first draft of the manuscript.

## Conference contributions

- I. Catalysis for ammonia production - fundamental studies towards passive-SCR systems**  
E C Adams\*, M Skoglundh and P-A Carlsson  
Oral presentation at *NordForsk network on catalyst design*  
2-3 June 2014, Tromsø, Norway
- II. Ammonia formation over supported platinum and palladium catalysts for passive-SCR applications**  
E C Adams\*, M Skoglundh, M Folic, P Gabrielsson, J Gustafson, L Merte, J Evertsson, C Zhang, M Shipilin, F Bertram and P-A Carlsson  
Oral-poster presentation at *8th International Conference on Environmental Catalysis*  
25-28 August 2014, North Carolina, USA
- III. Supported platinum and palladium catalysts for passive-SCR applications**  
E C Adams\*, M Skoglundh, M Folic, P Gabrielsson, J Gustafson, L Merte, J Evertsson, C Zhang, M Shipilin, F Bertram, D Dahl, M Laurell, H Schyllander and P-A Carlsson  
Oral presentation at *24th North American Catalysis Society Meeting*  
14-19 June 2015, North Carolina, USA
- IV. Elucidating the dependence on NO:H<sub>2</sub> ratios for ammonia formation over alumina supported platinum and palladium**  
E C Adams\*, M Skoglundh, E C Bendixen, P Gabrielsson, M Folic and P-A Carlsson  
Poster presentation at *10th International congress on catalysis and automotive pollution control*  
28-30 October 2015, Brussels, Belgium
- V. Cleaning poisonous gases from cars**  
E C Adams\*,  
Popular-science presentation at *Materials for tomorrow*  
3-4 November 2015, Gothenburg, Sweden
- VI. The chemistry of the palladium phase in Pd/Ce/Al<sub>2</sub>O<sub>3</sub> during ammonia formation**  
E C Adams\*, M Skoglundh, J Nilsson, N M Martin, G Agostini, O Mathon and P-A Carlsson  
Oral presentation at *9th International Conference on Environmental Catalysis*  
10-13 July 2016, Pennsylvania, USA

## Contents

<b>1</b>	<b>Introduction</b>	<b>1</b>
1.1	Automotive lean NO <sub>x</sub> abatement . . . . .	1
1.2	Passive selective catalytic reduction of NO <sub>x</sub> . . . . .	3
1.3	Objectives . . . . .	4
<b>2</b>	<b>Catalytic ammonia formation</b>	<b>5</b>
2.1	Heterogeneous catalysis . . . . .	5
2.2	The supported noble metal catalyst . . . . .	7
2.3	Ammonia formation pathways . . . . .	7
<b>3</b>	<b>Research approach and methods</b>	<b>9</b>
3.1	Sample preparation . . . . .	9
3.2	Physicochemical characterisation . . . . .	10
3.2.1	Sorption measurements . . . . .	10
3.2.2	X-ray diffraction (XRD) . . . . .	12
3.2.3	Elemental composition analysis . . . . .	13
3.3	Catalyst evaluation . . . . .	13
3.3.1	Flow-reactor measurements . . . . .	13
3.4	Time-resolved in situ characterisation . . . . .	14
3.4.1	Fourier transform infrared (FTIR) spectroscopy . . . . .	14
3.4.2	X-ray absorption spectroscopy (XAS) . . . . .	15
<b>4</b>	<b>Results and Discussion</b>	<b>17</b>
4.1	Influence of gas composition . . . . .	17
4.2	The role of catalyst formulation . . . . .	23
4.3	Catalyst structure-function relationship . . . . .	32
<b>5</b>	<b>Concluding remarks</b>	<b>37</b>

## List of abbreviations

<b>NO<sub>x</sub></b>	Nitrogen oxides, x = 1 or 2
<b>AFR</b>	Air-to-fuel ratio
<b>TWC</b>	Three-way catalyst
<b>LNT</b>	Lean NO <sub>x</sub> trap
<b>SCR</b>	Selective catalytic reduction
<b>AFC</b>	Ammonia formation catalyst
<b>BET</b>	Brunauer, Emmett, Teller
<b>OSC</b>	Oxygen storage capacity
<b>XRD</b>	X-ray diffraction
<b>ICP-OES</b>	Inductively coupled plasma optical emission spectroscopy
<b>MFC</b>	Mass flow controller
<b>CEM</b>	Controlled evaporator mixer
<b>FTIR</b>	Fourier transform infrared
<b>IR</b>	Infrared
<b>DRIFTS</b>	Diffuse reflectance infrared Fourier transform spectroscopy
<b>XAS</b>	X-ray absorption spectroscopy
<b>XANES</b>	X-ray absorption near-edge structure
<b>EXAFS</b>	Extended X-ray absorption fine structure
<b>WGS</b>	Water-gas-shift
<b>STEM-EDX</b>	Scanning transmission electron microscopy energy dispersive X-ray
<b>SMSI</b>	Strong metal-support interaction
<b>WLI</b>	White-line intensity

## 1.1 Automotive lean $\text{NO}_x$ abatement

The transport sector has been recognized as one of the main anthropogenic sources of atmospheric pollution and, as a sector, it has been rapidly growing since the 1970s [1, 2]. The number of passenger vehicles in the world is estimated to have grown from 748 to 907 million between 2009 and 2014 [3]. The increasing global demand on transport is an environmental concern due to the heavy reliance on fossil fuels. Not only are fossil fuels a finite source of energy, but their combustion also results in green-house gas emissions, *i.e.* carbon dioxide [4]. The high-pressure, high-temperature combustion processes associated with the use of hydrocarbon-based fuels also results in the formation of many harmful products including nitrogen oxides ( $\text{NO}_x$ , where  $x = 1$  or  $2$ ) [5]. The release of  $\text{NO}_x$  into the atmosphere results in numerous

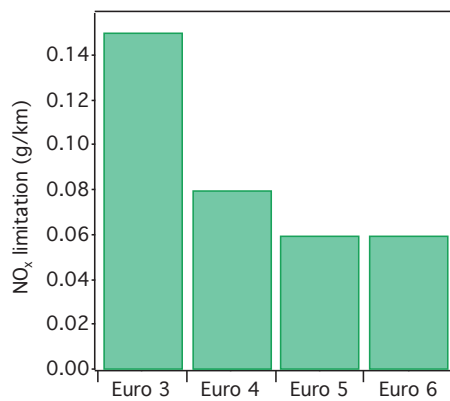
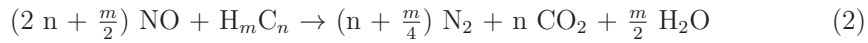
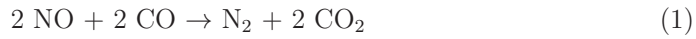


Figure 1.1: Maximum allowed emissions of  $\text{NO}_x$  from a gasoline fuelled passenger vehicle according to European Emissions Standards [6]

environmental effects including acid rain, smog formation and stratospheric ozone depletion [7]. When released into urban areas, biological effects are also seen in the form of cardiovascular and respiratory diseases, including asthma, bronchitis and pneumonia [8]. As a result of these implications, legislations regulating  $\text{NO}_x$  emissions are becoming increasingly stringent throughout Europe, Japan and the USA (See Figure 1.1 for European legislation standards [6]).

Vehicle fuel efficiency can be increased by employing lean-burn engines [9]. These engines operate at a higher air-to-fuel ratio (AFR) than the conventional stoichiomet-

ric engine,  $\lambda > 1$ , allowing the engine to utilise the fuel to a higher extent by facilitating more efficient combustion [10].  $\lambda$  represents the ratio between the actual engine AFR and the AFR at stoichiometric balance, i.e. when the mass of air consumed is just enough to burn all of the fuel. Whilst utilising lean-burn combustion concepts is beneficial for fuel economy, the activity for  $\text{NO}_x$  reduction over the conventional three-way catalyst (TWC) is diminished [11], as illustrated in figure 1.2. This is because carbon monoxide, hydrocarbons and hydrogen, which would ordinarily act as reducing agents for  $\text{NO}_x$  (see eqns 1-3) are rapidly converted to  $\text{CO}_2$  and  $\text{H}_2\text{O}$  in the presence of such strongly oxidizing conditions [12].



It is therefore imperative that techniques capable of efficiently handling  $\text{NO}_x$  in the presence of excess oxygen are developed. This is an extensive task because the conditions in which the after-treatment system should operate are extremely variable due to the different driving operations typically employed, e.g. cold starts, urban-driving etc. Temperatures commonly experienced in the exhausts of lean-burn gasoline vehicles can range between ambient and  $850^\circ\text{C}$  [12].

Lean  $\text{NO}_x$  trap (LNT) catalysts can be used to achieve a high cycle-averaged conversion of  $\text{NO}_x$  to  $\text{N}_2$  in net lean-burn vehicles [13]. For this technique, periodic cycling between long, lean (60 s) and short, rich operation (5 s), i.e. AFR above and below  $\lambda = 1$  is used [14]. During the lean cycle,  $\text{NO}_x$  is trapped on the storage component of the LNT catalyst, typically alkaline earth metals such as Ba or K. When the storage component becomes saturated, a brief rich cycle is necessary to convert the stored  $\text{NO}_x$  to  $\text{N}_2$  and regenerate the catalyst. Although commercially used in diesel vehicles, the higher  $\text{NO}_x$  concentrations and exhaust temperatures in lean-burn gasoline engines make the use of LNT systems challenging; Higher concentrations of engine-out  $\text{NO}_x$  means that more frequent regeneration of the LNT is required, resulting in an increased fuel penalty [15].

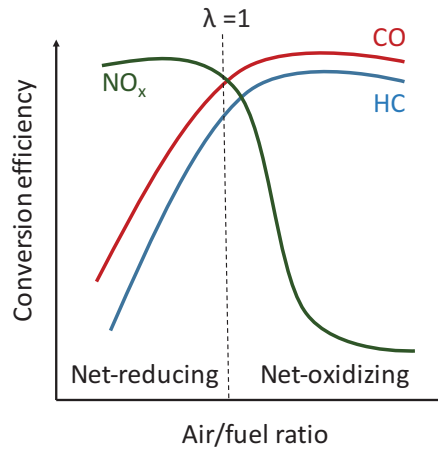


Figure 1.2: Representation of the catalytic conversion of  $\text{NO}_x$ , CO and hydrocarbons over the three-way catalyst as a function of air-to-fuel ratio

Selective catalytic reduction (SCR) of  $\text{NO}_x$  by  $\text{NH}_3$ , is an alternative technique capable of reducing  $\text{NO}_x$  in the presence of excess oxygen [16]. It is currently the preferred method for lean  $\text{NO}_x$  abatement on heavy duty vehicles and has been implemented on many buses and trucks throughout Europe and the USA [17]. Due to safety concerns with the toxicity, storage and transport of ammonia, this technology depends upon the use of a urea solution [18]. The urea is stored in a separate tank on-board the vehicle from where it is periodically injected into the exhaust when the addition of ammonia is required. In the high temperatures of the exhaust, the urea solution will thermally decompose and hydrolyse to form the required ammonia as well as  $\text{CO}_2$  [19, 20]. The use of the urea solution has several drawbacks related to temperature; it freezes below  $-11\text{ }^\circ\text{C}$ , slowly decomposes in the storage tank at temperatures above  $50\text{ }^\circ\text{C}$  and requires temperatures exceeding  $200\text{ }^\circ\text{C}$  in order to thermally decompose without the formation of any solid deposits [21, 22]. Although suitable for large heavy-duty vehicles, this method of after-treatment gives rise to some challenges when considering implementation in smaller vehicles, i.e. passenger cars. Ideally, the generation of an *onboard* supply of ammonia (rather than reliance on an external reductant such as the afore mentioned urea) has been suggested as an attractive, alternative means for lean  $\text{NO}_x$  reduction in passenger vehicles to meet the requirements of future  $\text{NO}_x$  emission legislations.

## 1.2 Passive selective catalytic reduction of $\text{NO}_x$

Passive-SCR is a proposed method for  $\text{NO}_x$  reduction in net lean-burn gasoline passenger vehicles. The underlying objective of this technique is to selectively reduce  $\text{NO}_x$  in the presence of excess oxygen by utilising a supply of  $\text{NH}_3$  that has been formed using gas components readily available in the exhaust stream. If sufficient amounts of ammonia can be formed, the need for an external reductant to be supplied and stored onboard the vehicle would no longer be necessary [23]. This is beneficial because there are several challenges associated with the use of urea solution with regards to implementing on small passenger vehicles compared to heavy-duty vehicles. These include, but are not limited to; the space required by the additional storage tank, the cost and complexity of the urea dosage system itself and the need for periodic customer intervention, although it has been reported that refilling the urea tank should only be required every 10,000 miles and so can be done during vehicle servicing [23, 24, 25, 26].

As with LNT systems, passive-SCR can be achieved by periodic cycling between lean and rich operation, i.e. AFR above and below  $\lambda = 1$ . Conceptually,  $\text{NH}_3$  can be formed over an ammonia formation catalyst (AFC) when short, rich pulses are made, by using  $\text{NO}_x$  and hydrogen-containing sources that are readily available within the exhaust stream. The formed  $\text{NH}_3$  is then stored on a suitable, underfloor SCR catalyst located downstream until said catalyst becomes fully saturated. Once the desired amount of  $\text{NH}_3$  is formed, the vehicle can return to lean operation, i.e. high fuel efficiency, and the stored  $\text{NH}_3$  is used to selectively reduce any  $\text{NO}_x$  that may breakthrough the AFC

during this period [24, 25, 26].

### 1.3 Objectives

This thesis treats the formation of ammonia from NO over supported heterogeneous catalysts that are relevant for passive SCR applications. The thesis objective is to deepen the understanding of how ammonia is formed from NO over noble metal based catalysts. In order to achieve this, a bottom-up research approach has been used with regards to the complexity of the reactions and catalyst formulations. Model catalysts with increasing complexity have been synthesised and evaluated using model gas feed reactions. An essential part of the studies has been to employ *operando* infrared and X-ray spectroscopic methods to reveal catalyst structure-function relationships.

## Catalytic ammonia formation

The formation of ammonia from  $\text{NO}_x$  has thus far been seen as a detrimental side reaction in automotive applications due to its toxicity and contribution to the production of secondary particulate matter [27]. It is thus not surprising that the vast majority of literature focusses upon how one can avoid its formation rather than promote it. In this chapter the phenomenon of catalysis will be introduced, followed by an overview of major routes by which ammonia can be formed.

### 2.1 Heterogeneous catalysis

By definition, a catalyst is a material that increases the rate of a chemical reaction without being consumed [28]. This is achieved by providing an alternative, lower energy pathway through which the elementary steps of a reaction can proceed (see figure 2.1) [29]. Catalysis is generally divided into two subgroups; homogeneous and heterogeneous. Homogeneous catalysis implies that the physical states of the reactants and catalytic material are the same. On the contrary, heterogeneous catalysis demands that the reactants are present in a different physical state from the catalytic material. In this thesis the reactants used are in the gas phase and are passed over a solid state catalyst. In industrial applications, heterogeneous catalysis is advantageous because the separation of catalyst and product is a relatively easy process [30]. Often, heterogeneous catalysts are also readily regenerated, recycled and have a long service life. Drawbacks however include higher sensitivity to poisoning and lower selectivity when compared to homogeneous catalysts [31].

The catalytic reaction involves adsorption of a reactant (or reactants) from the gas phase onto the catalyst surface, a process which lowers the potential energy of the system. Once adsorbed (molecularly or dissociatively), the reactant is able to diffuse across the catalyst surface, collide and react with other adsorbed atoms/molecules via the Langmuir-Hinshelwood mechanism. Principally, it is also possible for adsorbed atoms/molecules to react with incoming gas-phase molecules via the Eley-Rideal mech-

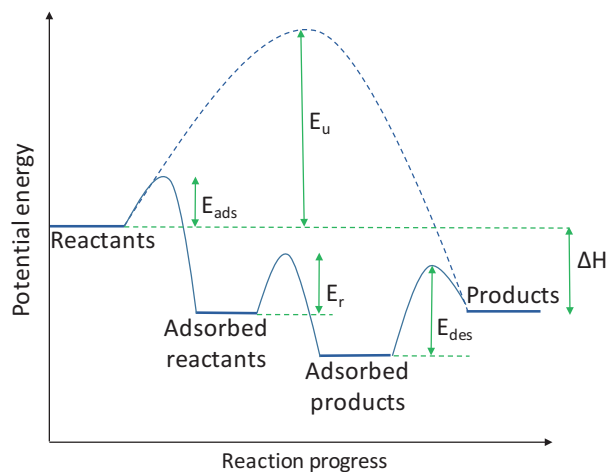


Figure 2.1: A simplified illustration of the catalytic cycle, comparing the activation energy barrier of the uncatalysed reaction ( $E_u$ ) in the gas-phase (dashed line) with the activation energy barriers associated with the alternative, multi-step catalytic reaction pathway (solid line), namely the adsorption ( $E_{ads}$ ) and reaction ( $E_r$ ) of reactants on the catalyst surface, before desorption ( $E_{des}$ ) of the formed products.  $\Delta H$  indicates the change in enthalpy between reactants and products.

anism, although this is far less common [32]. The reaction of adsorbed species is associated with a particular activation energy barrier. The energy required to overcome this barrier is significantly lower than that required by the uncatalysed reaction, i.e. reaction between gas phase molecules. For a particular reaction to occur, both steric, geometrical and electronic requirements must be met. When a reactant is adsorbed on a surface, rather than free in the gas phase, that reactant has one less degree of freedom; thereby increasing the likelihood of collision with another reactant. The formed product is then able to desorb from the catalyst surface via an endothermic elementary step [28]. It is noteworthy that the catalyst does not affect the amount of product formed, only the rate at which it is formed, thus the overall change in enthalpy from reactants to products is the same, whether or not a catalyst is used. In other words, although a catalyst is able to accelerate the rate of an elementary reaction step, once equilibrium is reached no gain is achieved by the addition of a catalyst. A reaction in equilibrium is under thermodynamic control, and the use of catalysts is only effective when the reaction is under kinetic control [32].

## 2.2 The supported noble metal catalyst

Throughout this work, model catalysts containing components commonly included in three-way catalyst (TWC) formulations have been focussed upon. This is because the current status of passive-SCR research suggests that suitable amounts of ammonia can be formed over TWCs during rich operation (low AFR) [15, 23, 24, 25, 26, 33, 34, 35], which will be discussed further below. However, TWCs have not been designed with optimising ammonia formation in mind, in fact a great deal of research has been conducted on its suppression. This work intends to investigate how TWC components can benefit ammonia formation activity.

In three-way catalytic converters, noble metal particles active for simultaneous oxidation of hydrocarbons and carbon monoxide, and reduction of  $\text{NO}_x$  must be distributed over a large surface area. Noble metals most commonly found in TWC formulations include platinum, palladium and rhodium [36]. The precious metals, often referred to as the active phase of the TWC, are supported on high surface area metal-oxides.  $\gamma$ -Alumina is the most commonly used support, due to its relatively high hydrothermal stability in the exhaust stream [12]. However, at excessive temperatures ( $> 1000$  °C), there is a risk of transformation of  $\gamma$ -alumina to  $\alpha$ -alumina which has a very low surface area [12]. To prevent the risk of this detrimental loss in surface area at high temperature, stabilizers such as silicon, barium and lanthanum are incorporated into the catalyst formulation [37]. Rare earth metal-oxides such as ceria are also incorporated to ensure high dispersion and prevent sintering of the active phase [37]. In automobiles, an effective method of ensuring high interaction between the gas phase and the catalyst without high pressure drop is the use of ceramic honey-comb structures, known as monoliths, on which the catalytic material can be coated [38]. This is required so that the mass transfer characteristics between the gas phase and the active catalyst surface are sufficient to allow desired catalytic conversion [39].

## 2.3 Ammonia formation pathways

### Reaction of $\text{N}_2$ with $\text{H}_2$

The catalytic synthesis of  $\text{NH}_3$  from  $\text{N}_2$  and  $\text{H}_2$ , known as the Haber-Bosch process, is a reaction which has been industrially utilised for over 100 years [40]. During this reaction, gaseous  $\text{N}_2$  and  $\text{H}_2$  are dissociatively adsorbed onto a catalyst surface (classically Fe-based) [41].  $\text{NH}_3$  can then be formed by stepwise addition of H adatoms to an N adatom before desorption from the catalyst surface.  $\text{N}_2$  is a highly stable molecule, due to the strength of its triple bond, nonpolarity and high ionization potential [42]. Therefore, the activation of  $\text{N}_2$  on the catalyst surface is an energy intensive process, demanding temperatures and pressures between 350 - 550 °C and 150 to 350 atm respectively [43]. The high pressure conditions required for this reaction to take place is, not only energetically unfavourable, but unsuitable for consideration onboard

passenger vehicles. For these reasons, nitrogen from the air is not deemed suitable as a reactant from which to form  $\text{NH}_3$  for this application.

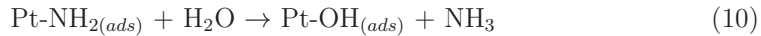
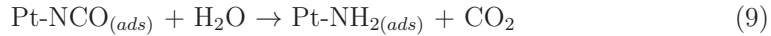
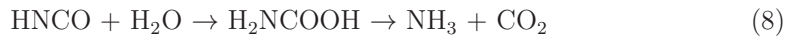
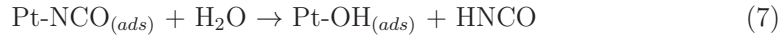
### Reaction of NO with $\text{H}_2$

Since the development of the TWC in the early 70s,  $\text{NH}_3$  formation has been considered a side-reaction of  $\text{NO}_x$  reduction that should be suppressed due to its toxicity and contribution to the production of secondary particulate matter [44, 45]. In particular, platinum and palladium-based catalysts were identified as having high selectivity towards  $\text{NH}_3$  in the presence of NO and  $\text{H}_2$  [46, 47, 48]. The formation of ammonia is observed provided that the  $[\text{H}_2]/[\text{NO}]$  ratio  $\geq 2.5$  is fulfilled. If this stoichiometry is not met, selectivity to other products including  $\text{N}_2\text{O}$  and  $\text{N}_2$  is preferred (see eqns 4-6):



### Isocyanate hydrolysis route

In 1973, Unland studied the reaction of NO with CO on noble metal catalysts for automobiles [49, 50]. The author saw the presence of absorption bands characteristic for surface isocyanate species using infrared spectroscopy and the intensity of these bands correlated to the ammonia formation activity of the materials being tested. It was therefore suggested that the hydrolysis of isocyanate species could lead to the formation of  $\text{NH}_3$ . The formation of isocyanate groups on the catalyst surface was further investigated by Solymosi *et al.*, who identified that it can take place in two ways, depending on the reaction temperature [51]. At high temperature (300 - 400 °C) the formation of isocyanates proceeds via the reaction between gaseous CO and adsorbed N formed during the dissociative adsorption of NO. At low temperature however, the formation proceeds via the reaction between gaseous CO and adsorbed NO, leading to its dissociation. Once formed, the isocyanate group is rapidly hydrolysed to ammonia via the following reactions (eqns 7-10) [52]:



Equations 4 - 10 will be frequently referred to throughout this work as they are highly relevant to the feed gas compositions investigated.

## Research approach and methods

### 3.1 Sample preparation

Supported noble-metal catalysts were investigated in this work. The incipient wetness impregnation technique was used for the preparation of all samples. This technique, also known as dry impregnation, is one of the most common preparation methods used in industry due to its relative simplicity and the minimization of metal salt waste [53]. Support materials were thermally treated in air at 600 °C prior to impregnation in order to remove impurities and stabilise the structure. The saturation point of each support was determined and the corresponding volume of aqueous solutions containing the relevant noble metal precursor was prepared. The pH of the solution was adjusted in order to increase the electrostatic interaction between the support material and the metal precursor [1]. The solution was then added dropwise, with stirring to the support material and the resultant paste was instantly frozen with liquid nitrogen and freeze-dried for approximately twelve hours. The use of freeze-drying, as opposed to oven-drying, ensures that the porous structure of the support material does not collapse during solvent removal because it is removed via sublimation rather than boiling [54, 55]. A further benefit of freeze-drying is that finely dispersed metal clusters are less likely to migrate. When oven-drying is used, these small clusters may migrate to the pore edges and agglomerate to form larger particles (see Figure 3.1). The dried samples were then calcined in air at 550 °C for one hour.

For use in the flow-reactor, the prepared powder catalysts were coated onto cordierite monolith substrates using a dip-coating technique. The powder catalysts and suitable binder materials (based on support composition) were suspended in a water-ethanol mixture to form a slurry. The monolith was then immersed into the slurry, allowing the catalyst-containing suspension to fill the channels by capillary forces. The monolith was then dried gently in air at 90 °C for two minutes, followed by calcination at 600 °C for two minutes. This process was repeated until the desired mass of washcoat was applied to the monolith. As a final step, the coated monoliths were then calcined in air at 600 °C for two hours.

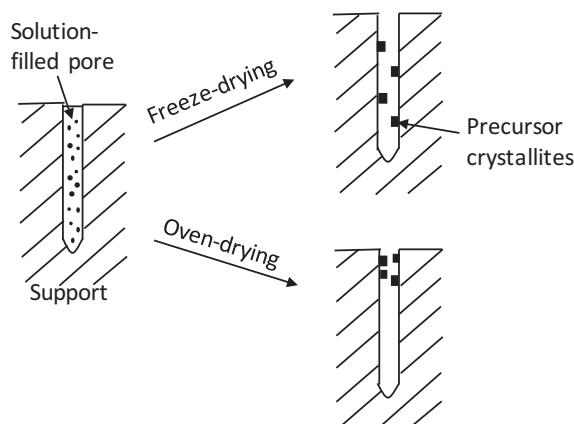


Figure 3.1: Schematic of how the dispersion of precursor crystallites in the pores of the support material can be affected by the choice of drying method during synthesis.

## 3.2 Physicochemical characterisation

### 3.2.1 Sorption measurements

#### Nitrogen physisorption

The physisorption of an inert gas, in this case nitrogen, can be used to determine the total surface area of mesoporous samples in accordance with theory put forward by Brunauer, Emmett and Teller, the so-called BET method [56]. The theory, which is an extension of Langmuir theory for monolayer adsorption, includes the treatment of multilayer adsorption and assumes that; (i) the rate of adsorption and desorption in any layer are equal, (ii) in the first layer, molecules adsorb on equivalent sites, (iii) molecules in the  $n^{\text{th}}$  layer constitute the adsorption sites for molecules in the  $(n+1)^{\text{th}}$  layer, and (iv) adsorption at one site does not affect adsorption at neighbouring sites [28, 57]. Taking these assumptions into account, the number of nitrogen molecules needed to form a complete monolayer over the sample can be determined.

Practically, the measurement is performed by heating the sample under vacuum to remove any surface moisture, followed by cooling to  $-196\text{ }^{\circ}\text{C}$  which is equivalent to the boiling point of nitrogen. The amount of nitrogen physisorbed onto the sample ( $V$ ) as a function of pressure is then measured at relative pressures,  $P/P_0$ , between 0.05 - 0.20.  $P$  is the equilibrated pressure and  $P_0$  is the saturation vapour pressure of  $\text{N}_2$  at  $-196\text{ }^{\circ}\text{C}$ . At low partial pressure, the relationship between  $P/V(P_0 - P)$  and  $P/P_0$

is linear. The volume of nitrogen required to form a monolayer on the sample ( $V_m$ ) is determined from the slope and intercept of the straight-line curve obtained when  $P/V(P_0 - P)$  is plotted against  $P/P_0$ , according to the BET equation (11) [58]:

$$\frac{P}{V(P_0 - P)} = \frac{C - 1}{V_m C} \frac{P}{P_0} + \frac{1}{V_m C} \quad (11)$$

Once  $V_m$  is quantified, the ideal gas law can be used to calculate the number of adsorbed nitrogen molecules. Multiplying the number of molecules adsorbed by the cross-sectional area of  $N_2$  ( $0.162 \text{ nm}^2$ ) gives the total surface area of the sample.

### Selective chemisorption

The purpose of selective chemisorption is to determine the noble-metal dispersion of the prepared catalyst. Dispersion is defined as the ratio between the number of exposed surface metal atoms and the total number of metal atoms in the sample. In this work, the characterisation is performed by sequential exposure of the samples to two pulses of CO at room temperature ( $25 \text{ }^\circ\text{C}$ ) whilst measuring the outlet concentration with a mass spectrometer. After the first pulse, when total uptake of CO occurs over the sample, Ar is flushed for 15 minutes. This ensures the removal of weakly bound CO from the sample surface prior to the second CO pulse which measures the reversible CO uptake. To quantify the number of surface metal atoms in the sample, the difference between the total and reversibly adsorbed CO is then calculated. In order to clean the surface of preadsorbed carbonaceous species before the measurement is performed, the sample is heated to  $500 \text{ }^\circ\text{C}$  in excess oxygen. The sample is then reduced in  $H_2$  at  $500 \text{ }^\circ\text{C}$ , before cooling to room temperature in Ar. Ceria-containing samples were pretreated with  $CO_2$  at room temperature, in order to selectively saturate the surface of the ceria component and ensure CO chemisorption is localised to the palladium phase [59]. Although a seemingly simple technique, in practice the exact stoichiometry between the total number of chemisorbed CO molecules and the number of surface palladium metal atoms varies between one and two, as chemisorption of both linear and bridge-bonded species is possible [60]. In this work, a CO: Pd ratio of 1:1 has been used so as not to overestimate the dispersion of the samples. This ratio was used for comparison of the dispersion for in-house prepared samples only, as opposed to comparison with literature.

### Oxygen storage capacity (OSC) measurements

Characterising the storage and release of oxygen from the samples in the presence of lean and rich environments respectively was necessary for understanding the behaviour of the samples under transient reaction conditions. The so-called 'dynamic'

OSC of each sample was determined by sequential injection of CO/Ar and O<sub>2</sub>/Ar, which was repeated for ten cycles so as to obtain a consistent catalyst response. The availability of surface oxygen species under transient conditions, as opposed to 'total' OSC which also includes the bulk, was focussed on in this work because the immediate availability of surface-oxygen is important when considering materials for automotive applications where rapid switches between lean and rich environments occurs. After pulsing of oxygen, Ar was flowed over the sample in order to remove any weakly-bound oxygen from the catalyst surface. Then, when CO was introduced and reacted with stored oxygen, the amount of CO<sub>2</sub> formed was detected by use of a mass spectrometer.

### 3.2.2 X-ray diffraction (XRD)

XRD is a non-destructive technique for identification of crystalline phases within the sample. It is performed by directing monochromatic X-rays onto the sample at an angle ( $\theta$ ), whereupon the beam will be scattered in a pattern characteristic to the bulk structure of the material. In order for an X-ray to diffract, the spacing between atom layers of the sample ( $d$ ) must be close to the radiation wavelength ( $\lambda$ ). Constructive interference occurs when beams diffracted by two different layers are in phase, giving rise to a peak in the diffraction pattern according to Bragg's Law (eqn 12):

$$n\lambda = 2d \sin\theta \quad (12)$$

If destructive interference occurs, and the diffracted beams are out of phase, no diffraction peak will occur. In this work, a Bruker D8 Advance powder X-ray diffractometer with monochromatic CuK <sub>$\alpha$ 1</sub> radiation was used. The incident beam angle was varied between 15-85° with a step size and time of 0.041° and 1 s respectively.

Although not quantitatively used in this work, it is also possible to use the peak width of an obtained XRD pattern to give an indication of crystallite size. The Scherrer equation (eqn 13) relates the width of a powder diffraction peak to the average dimensions of crystallites [29]:

$$B(2\theta) = \frac{K\lambda}{L\cos\theta} \quad (13)$$

Where the peak width,  $B(2\theta)$ , is inversely proportional to the crystallite size,  $L$ . The constant,  $K$ , is related to the crystallite shape and is generally assumed to be 1 for spherical particles.

### 3.2.3 Elemental composition analysis

The elemental composition of a material can be determined by a variety of methods. In this work, inductively coupled plasma optical emission spectroscopy (ICP-OES) has been used in this work to quantify the total elemental composition of prepared catalysts. The sample was first digested in a solution of nitric and hydrochloric acid, resulting in a clear sample solution. The solution is then accelerated as an aerosol through a high-temperature plasma-fireball, whereupon it loses molecular association and the sample elements are ejected as free atoms or ions [61]. As they cool, the atoms/ions relax to their ground state and emit characteristic spectral lines, which can be compared to the signal from certified calibration standards in order to quantify their amounts.

## 3.3 Catalyst evaluation

### 3.3.1 Flow-reactor measurements

A flow-reactor (schematic shown in Figure 3.2) was used to examine the catalytic activity of the prepared samples. The reactor setup consists of a mounted quartz tube which is surrounded by a metal coil which is heated in a controlled manner by use of a temperature regulator. The washcoated monolith is placed inside the tube, with an uncoated (blank) monolith placed on either side of the sample in order to minimize heat losses by radiation and thus preserve a constant temperature both axially and radially throughout the sample [62]. Two thermocouples (type K) are positioned in the reactor. The first measures the temperature in the middle of the sample-coated monolith, whilst the second is placed  $\sim 10$  mm upstream of the sample and is used to control the temperature of the reactor. The inlet gas composition was controlled using separate mass flow controllers (MFCs, Bronkhorst) and the total flow was kept constant throughout the course of each reaction by use of balance Ar. Liquids could be fed to the reactor via a controlled evaporator mixer (CEM, Bronkhorst) system. The CEM system consists of both a liquid MFC for the water/HC of choice, and a gas MFC for Ar carrier gas. These MFCs are connected to a small furnace, in which the liquid can be vaporized and carried to the reactor inlet via heated tubing. The reactor outlet composition was analyzed by an internally calibrated gas-phase Fourier transformed infrared (FTIR) spectrometer (MKS 2030) and, in some cases a mass spectrometer is also used.

Prior to all experiments, the sample is pretreated with  $O_2$  (2 vol.%) at 500 °C for 30 minutes. Throughout this work, the flow-reactor was used for steady-state activity measurements, temperature-programmed ramp experiments and transient cycling between lean and rich environments.

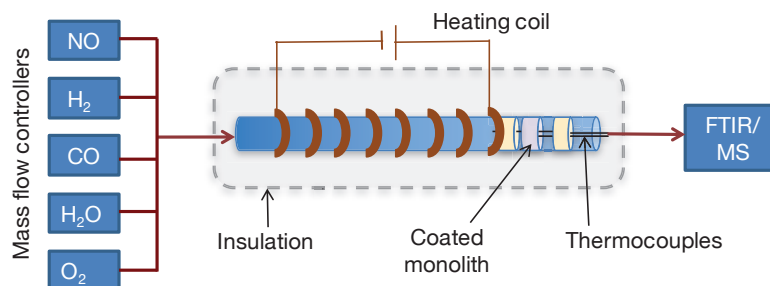


Figure 3.2: Schematic of the flow reactor system employed throughout this work. Red arrows indicate the direction of the gas-flow.

## 3.4 Time-resolved in situ characterisation

### 3.4.1 Fourier transform infrared (FTIR) spectroscopy

Infrared (IR) spectroscopy is one of the most widely used tools in surface science and catalysis research [63]. It is an efficient method for characterising reactants and intermediate species adsorbed on the catalyst surface as well as products in the gas phase. Molecules possess discrete levels of rotational and vibrational energy. IR spectroscopy relies on the transition between vibrational energy levels by the absorption of photons with frequency in the mid-infrared range ( $200 - 4000 \text{ cm}^{-1}$ ). Molecules contain bonds of specific energy and spatial orientation and, when energy is supplied to such bonds, they may bend, stretch or distort [61]. In order for an infrared photon to be absorbed by the molecule, a change in dipole moment must occur during the vibration, rendering it IR active. The intensity of the infrared band observed is proportional to this change in dipole moment and is therefore characteristic to that particular molecule. Vibrational frequencies increase with increasing bond strength and decreasing mass of the vibrating atom [64].

In this work, *in situ* IR characterisation has been carried out in diffuse reflectance infrared Fourier transform (DRIFT) mode for identification of surface-bound molecular species during ammonia formation. An added benefit of this method of scanning is the ability to work with powder samples, as opposed to the preparation of wafers, usually used in transmission FTIR. This, not only avoids the need for any complicated preparation procedure, but also ensures that diffusion of gas through the sample is not

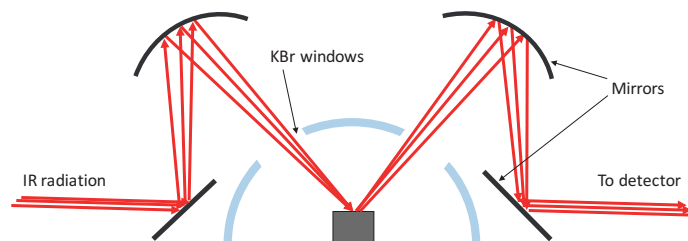


Figure 3.3: Schematic of diffuse reflectance infrared spectroscopy measurement setup.

limited, as may be the case when testing a wafer. A schematic of the DRIFTS setup is shown in Figure 3.3.

The focussed infrared beam is directed onto the sample cup using an ellipsoidal mirror, and is subsequently absorbed, transmitted and reflected by the sample. The diffusively reflected radiation is then collected by a second ellipsoidal mirror and directed towards a suitable detector. A fingerprint spectrum, characteristic of specific adsorption sites and adsorbed species, is then generated for analysis.

### 3.4.2 X-ray absorption spectroscopy (XAS)

X-ray absorption spectroscopy can be used to analyse the chemical state and local environment of a given element, without the need for long-range order in the sample or low-pressure environments [63]. The experiment is performed by stepwise exposure of the sample with X-rays of a specific energy. Some of the X-rays will be absorbed by the atoms in the sample, resulting in the excitation or ejection of a core electron to excited electronic states or the continuum. By comparing the intensity of the beam before and after it is passed through the sample, the absorption can be quantified. After repeating this process over the energy range of interest, an X-ray absorption spectrum can be produced. A typical spectrum is displayed in Figure 3.4.

The sudden increase in absorption is known as the absorption edge and corresponds to the energy required for excitation of the core electron described above. The spectrum can usually be separated into two distinct regions; the X-ray absorption near-edge structure (XANES) and the extended X-ray absorption fine structure (EXAFS) regions. The XANES region can provide information regarding the oxidation state and coordination environment of the metal atom, whilst the EXAFS region can be used to determine the radial distribution of atoms around the absorbing atom [65].

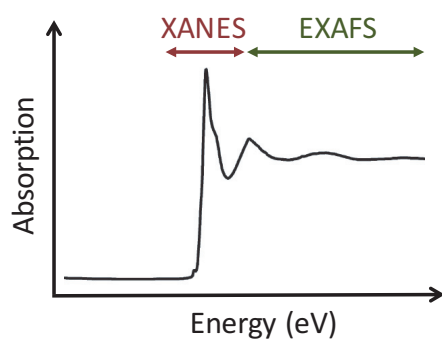


Figure 3.4: Representation of a normalized X-ray absorption spectrum.

In this work, *in situ* XAS has been performed to investigate changes in the noble-metal oxidation state and coordination number during the formation of ammonia from NO and H<sub>2</sub>. Particular focus has been directed towards the effect of O<sub>2</sub> on the reaction.

## Results and Discussion

### 4.1 Influence of gas composition

In this work, the activity for ammonia formation over noble-metal catalysts in various reaction environments has been studied. This includes the comparison of ammonia formation from nitric oxide when a direct supply of hydrogen is available in the feed and whether water could be a viable source of hydrogen for ammonia formation. The use of water was investigated as it is a byproduct of the combustion process and hence abundant in the exhaust stream of automobiles. The effect of oxygen on the reaction was investigated for several reasons. As discussed in section 1, passive-SCR is a technique which relies on periodic switching between rich and lean operation. If  $\text{NH}_3$  can be formed efficiently over the AFC in near-stoichiometric conditions, the fuel penalty obtained as a result of operating in the rich regime can be minimized. Conversely, if a delay in  $\text{NH}_3$  formation occurs after switching to rich operation and AFC activity is low, resulting in longer periods of time necessary for the downstream SCR to be saturated with stored  $\text{NH}_3$ , the resultant fuel penalty will be considerable [25]. More complex mixtures have also been tested to investigate ammonia formation in multi-component feed gas compositions relevant to those one would encounter onboard a lean-burn gasoline vehicle. In this section, general trends in results are discussed with the prime focus on gas phase stoichiometry.

#### The $[\text{H}_2]:[\text{NO}]$ ratio and reaction temperature

As discussed in section 2.3, the molar ratios of hydrogen and nitrogen oxide determines the selectivity towards specific nitrogen-containing products at intermediate reaction temperature. In paper I, the influence of this ratio on selectivity and surface speciation was investigated at both low (150 °C) and intermediate (350 °C) temperatures. Figure 4.1a shows that, at intermediate temperature, the selectivity to specific N-containing products follow the stoichiometry laid out in equations 4, 5 and 6 (section 2.3). As the concentration of  $\text{H}_2$  in the feed increases, the selectivity shifts from  $\text{N}_2\text{O}$  (in addition to significant NO slip) to  $\text{N}_2$ , before 100 % conversion to  $\text{NH}_3$  is observed when the

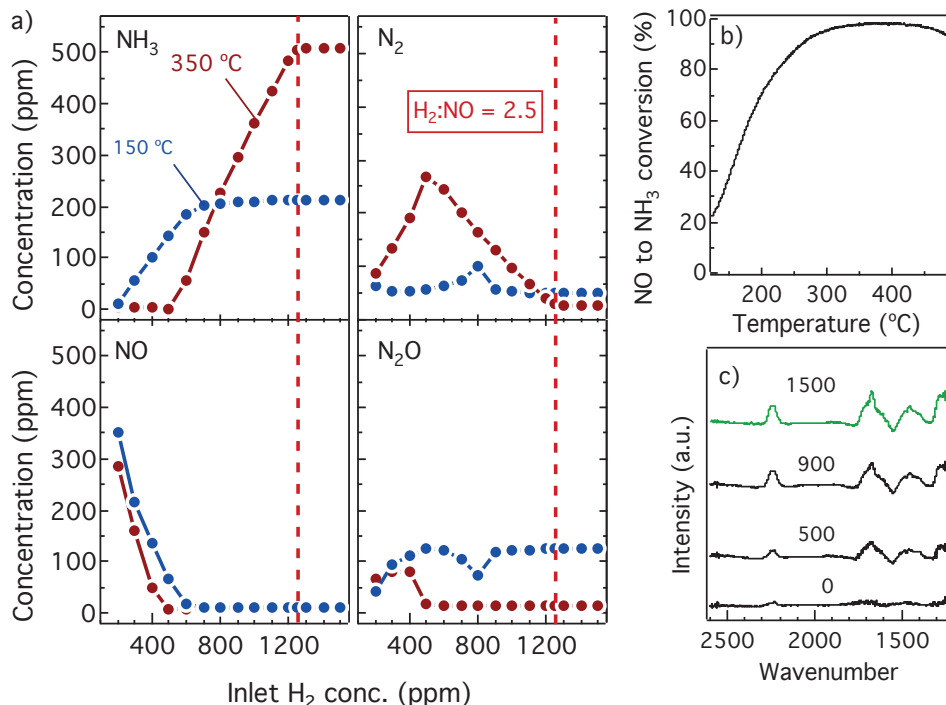


Figure 4.1: *Left-panel:* a) Steady-state formation/slip of NH<sub>3</sub>, N<sub>2</sub>, NO and N<sub>2</sub>O over Pd/Al<sub>2</sub>O<sub>3</sub> at 150 °C (blue) and 350 °C (red) versus the concentration of H<sub>2</sub> in the feed. The NO concentration was constantly 500 ppm throughout the reaction. b) Conversion of NO to NH<sub>3</sub> versus reactor temperature in the presence of NO + H<sub>2</sub> ([H<sub>2</sub>]:[NO] = 2.5) and (f) DRIFT spectra acquired during H<sub>2</sub> dependence experiments at 150 °C. The H<sub>2</sub> concentrations are displayed on the spectra and the green spectrum indicates a [H<sub>2</sub>]:[NO] ratio > 2.5.

[H<sub>2</sub>]:[NO] ratio > 2.5. However, when the temperature is low and the required amount of H<sub>2</sub> is provided for selectivity to NH<sub>3</sub>, the maximum conversion to NH<sub>3</sub> achieved over the sample was 50%.

Temperature dependence was confirmed in Paper II where temperature programmed experiments were performed to determine the active temperature window for ammonia formation over selected catalysts (Figure 4.1b). It was seen that complete conversion to NH<sub>3</sub> is possible when the catalyst inlet temperature is above 275 °C. The low NH<sub>3</sub> formation activity at 150 °C is explained by self-poisoning by NO on the catalyst surface. Upon observation of the DRIFT spectra in Figure 4.1c, a prominent contribution from nitrogen-containing surface species was observed at low temperatures. The buildup of NO<sup>+</sup> at low temperature occurs because the reactant adsorbs associatively onto the active sites of the catalyst. At this temperature, H<sub>2</sub> is required to facilitate the N-O bond

scission via the formation of an HNO intermediate group [66, 67, 68]. The difficulty in dissociating NO over the catalyst at low temperature is evidenced in Figure 4.1a, where it is observed that despite increasing the concentration of H<sub>2</sub> available for reaction, a near-constant formation of N<sub>2</sub>O is observed over the sample at low temperature. This indicates that, although NO dissociation still occurs, the surface recombination of NO with N adatoms is almost as likely as the recombination of N and H adatoms.

### Water-gas-shift assisted ammonia formation

Since the ideal [H<sub>2</sub>]:[NO] ratio of 2.5 may not always be available in the vehicle exhaust stream, water was investigated as a viable source of hydrogen for ammonia formation. As CO is also present in the exhausts during rich engine operation, the water-gas-shift reaction (eqn 14) was exploited in Papers II, III and IV by investigating feeds containing NO, CO and H<sub>2</sub>O.



However, NH<sub>3</sub> can also be formed via hydrolysis of isocyanate groups as previously discussed (eqns 7-10, section 2.3). Thus, when CO and H<sub>2</sub>O are present in the reaction feed, there are two potential routes through which the formation of NH<sub>3</sub> could proceed. Indeed, Paper IV shows that, at temperatures below 200 °C, hydrolysis of isocyanates is the dominant route for NH<sub>3</sub> formation. This was concluded because, when the WGS activity of the sample was tested in the absence of NO, the amount of H<sub>2</sub> formed was not sufficient to supply the necessary amounts of hydrogen required for the ammonia formed at the same temperature upon the addition of NO to the feed

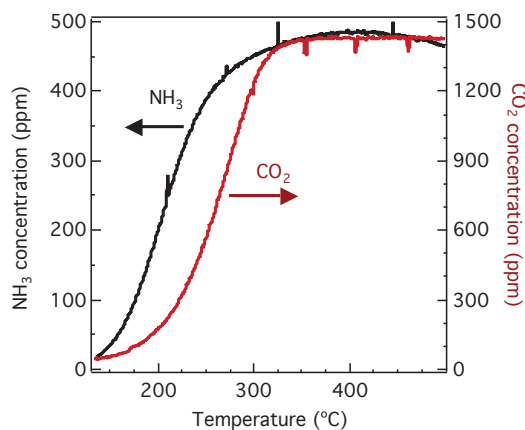


Figure 4.2: NH<sub>3</sub> formation over Pd/Ce/Al<sub>2</sub>O<sub>3</sub> in the presence of 500 ppm NO, 1500 ppm CO + 2 vol.% H<sub>2</sub>O (black line) and CO<sub>2</sub> formation via the water-gas-shift reaction in the presence of 1500 ppm CO + 2 vol.% H<sub>2</sub>O (red line) versus catalyst inlet temperature. Ar balance employed, space velocity = 40,000 h<sup>-1</sup>

(displayed in Figure 4.2). The formation of  $\text{CO}_2$  was monitored as an indicator of the activity for the WGS reaction. From the stoichiometry in equation 14,  $\text{CO}_2$  and  $\text{H}_2$  are formed in equivalent amounts (1:1). This shows that even whilst using 'simplistic' model feed compositions, the chemistry governing ammonia formation from nitrogen oxide is complex.

### The impact of oxygen

As described in section 1.2, passive-SCR is reliant on periodic switching between rich and lean conditions. During lean conditions, a large excess of oxygen is present, having a significant effect on reaction selectivity and ammonia formation activity. In this work, transient experiments have been conducted, where periodic pulses of oxygen are admitted into the reaction mixture being tested, to simulate the cycling observed in passive-SCR. The results of these tests will be discussed in section 4.2 as they are often very dependent on the catalyst being tested. Instead, this section will focus on so-called oxygen-sweep experiments. For these experiments, the concentration of  $\text{O}_2$  fed to the reactor was altered, focusing on concentrations close to the stoichiometric point (balanced concentration of oxidizing and reducing agents) of the reaction feed. This was done to gain insight into how rich the exhaust stream must be before suitable amounts of ammonia can be formed over the respective AFCs. The stoichiometric value (S) of the feed characterizes the net oxidizing-reducing character of the inlet feed and is calculated according to the following equation (eqn 15) [69]:

$$S = \frac{2[\text{O}_2] + [\text{NO}]}{[\text{CO}] + [\text{H}_2] + 9[\text{C}_3\text{H}_6]} \quad (15)$$

Calculated S-values less than 1 represent gas mixtures which are net-reducing in character. When S is equal to 1, the fed stream is at the stoichiometric point, whilst feeds resulting in S-values above 1 are net-oxidizing.

Oxygen-sweep experiments in Paper II showed that, for the investigated catalysts,  $\text{NH}_3$  is formed only when feed mixtures are net-reducing in nature (Figure 4.3a). When net-oxidizing conditions are available, the formation of  $\text{NH}_3$  is suppressed entirely. Slip of NO is observed over the catalyst when  $S > 1$ , the concentration of which increases as the feed becomes increasingly oxidizing. The loss in activity in the presence of oxidizing feeds is due partly to the oxidation of reductant, but also as a result of chemical changes to the noble metal phase of the catalyst itself which will be discussed further in section 4.3. Flow reactor experiments showed that, when the feed contains a direct source of hydrogen, *i.e.*  $\text{H}_2$ , total oxidation of the reductant to water occurs when  $S > 1$ , thereby limiting the formation of ammonia over the sample.

The oxidation of the supplied reductant was also observed during *in situ* DRIFTS analysis, where altering the  $\text{O}_2$  concentration of the reaction feed impacted surface-species coverage during the WGS-assisted experiment (Figure 4.3b). A significant IR

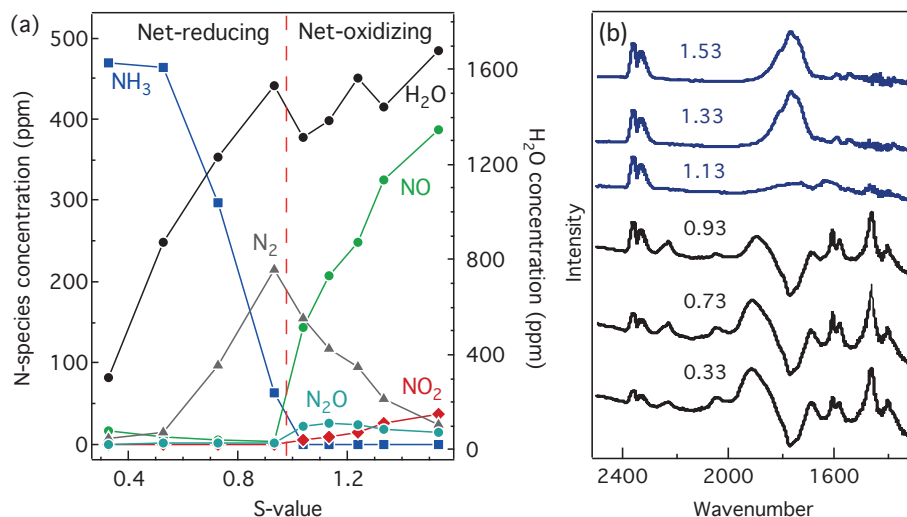


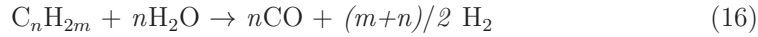
Figure 4.3: (a) Steady-state formation/slip of NH<sub>3</sub>, NO, N<sub>2</sub>, NO<sub>2</sub>, N<sub>2</sub>O and H<sub>2</sub>O over Pd/Al<sub>2</sub>O<sub>3</sub> at 350 °C versus the stoichiometric-value of the feed. The feed consisted of constant supply of NO (500 ppm) + H<sub>2</sub> (1500 ppm) whilst the concentration of O<sub>2</sub> was varied between 0 and 1050 ppm, corresponding to S-values between 0.33 and 1.73. Ar balance employed, space velocity = 40,000 h<sup>-1</sup>. (b) DRIFT spectra acquired at 350 °C with inlet concentration of 500 ppm NO, 1500 ppm CO and 2 vol.% H<sub>2</sub>O. O<sub>2</sub> concentration was varied between 0 and 1050 ppm (S = 0.33 - 1.53) and Ar balance was employed.

absorption band, representative of gaseous CO<sub>2</sub> (2350 cm<sup>-1</sup>) was observed in the presence of excess oxygen. As the concentration of O<sub>2</sub> in the feed decreases, the contribution of the CO<sub>2</sub> band decreases and the intensity of both bridged and linearly-bound CO (1936 and 2070 cm<sup>-1</sup> respectively) increases simultaneously. The increase in CO adsorption is accompanied by an increasing contribution from bands in the NH stretching region (not shown here), relating to an increase in the amount of surface bound NH<sub>3</sub>. This indicates that, in the presence of excess oxygen, CO is preferentially oxidized to form CO<sub>2</sub> rather than undergoing the WGS reaction to form the hydrogen required for ammonia formation.

### Reaction in the presence of complex model feed mixtures

The activity for ammonia formation using complex model feeds containing reactants relevant to those one would encounter onboard a lean-burn gasoline vehicle [25] was investigated in Paper V. For this study, CO<sub>2</sub> and H<sub>2</sub>O were present in excess, in addition to C<sub>3</sub>H<sub>6</sub>, CO, H<sub>2</sub>, NO and O<sub>2</sub>, the concentrations of which corresponded to specific S-values. As a result of hydrocarbon addition to the feed, an additional pathway for

hydrogen formation is available, namely steam-reforming (eqn 16):



In Figure 4.4 it is seen that the highest concentrations of ammonia are always formed at the richest S-values. This trend was seen to be independent of the catalyst formulation. The theoretical maximum concentration of  $NH_3$  possible under the reaction conditions employed in this experiment is 1500 ppm. The ammonia formation decreases as feeds become increasingly oxidizing, becoming entirely suppressed under stoichiometric conditions ( $S = 1$ ). As this study was conducted at 500 °C, it is likely that both WGS and steam reforming reactions take place and are able to provide hydrogen for ammonia formation in the reducing conditions ( $S < 1$ ). As neither  $NO$ ,  $NO_2$  nor  $N_2O$  were detected at the reactor outlet when  $S < 1$ , it is assumed that  $N_2$  is the only other N-containing product formed over the samples.

The increase in CO concentration, as the feed becomes more reducing in nature, correlates with the ammonia formation behaviour of the samples. This trend has been reported in other passive-SCR studies and is thought to be due to partial oxidation or steam reforming of the propene in the feed, as opposed to slip of the inlet CO over the sample [25, 26]. This is undoubtedly a concern for passive-SCR applications since CO is also a regulated emission.

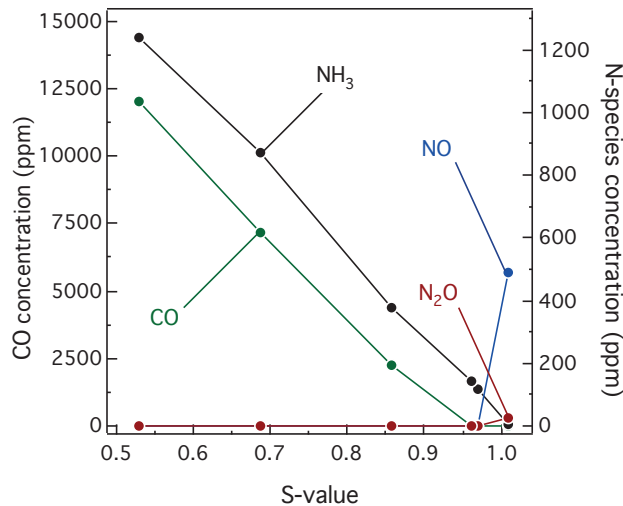


Figure 4.4: Outlet concentrations of  $NH_3$ ,  $CO$ ,  $NO$  and  $N_2O$  measured over  $Pd/Ce/Al_2O_3$  at 500 °C in various rich feed gas compositions ( $S < 1$ ). The concentrations of  $NO$ ,  $CO$ ,  $H_2$ ,  $C_3H_6$ ,  $CO_2$  and  $H_2O$  fed were held constant, whilst the concentration of  $O_2$  was varied between 0.79 and 1.59 vol.% corresponding to S-values between 0.529 and 0.970.  $GHSV = 20,000 h^{-1}$  and Ar balance employed.

## 4.2 The role of catalyst formulation

Components commonly found in TWC formulations were investigated throughout this work. A bottom-up approach was taken with regards to catalyst composition by initially focussing on noble metal and support effects, before adding complexity in the form of a third component. Finally, activity of model samples were compared to that of a commercially-available TWC in order to identify any further trends in behaviour that were not seen by in-house prepared samples.

### Comparison of platinum- and palladium-based catalysts

In Paper II, the activity of platinum and palladium based catalysts was compared with regards to ammonia formation via a direct source of hydrogen and also using hydrogen supplied in the form of water. In order to make an objective comparison of the noble metal phase, the molar equivalent of platinum and palladium was used in the preparation of the samples. This ensured that the number of metal atoms in each catalyst was approximately the same, corresponding to a loading of 1.0 and 0.5 wt.% Pt or Pd respectively. The targeted loading was confirmed by ICP-OES and, for the alumina supported samples discussed in this section, showed that the desired noble metal content was achieved within a  $\pm 0.07$  wt.% tolerance. Of course, the number of metal atoms is not the only criterion which affects catalytic activity as characteristics such as dispersion, particle size distribution and geometric configuration also play an important role [70].

Flow-reactor experiments showed that the type of noble-metal employed in the catalyst formulation has a significant effect on the temperature required for 50 % conversion of the fed NO to NH<sub>3</sub> ( $T_{50}$ ). It was also seen that the benefit of using platinum/palladium for one reaction, was not necessarily beneficial when used for alternate reactions. For example, whilst performing temperature-programmed experiments from 500 to 150 °C, to evaluate catalytic activity as a function of catalyst inlet temperature,  $T_{50}$  was lower for Pt-based samples in feeds when hydrogen was directly available, whilst  $T_{50}$  for Pd-based samples was lower during the WGS-assisted reaction (Figures 4.5a and b respectively). However, once the temperature exceeded 300 °C, the Pt containing catalysts were the most active samples in both reaction environments. The enhanced low-temperature WGS activity over Pd is a phenomenon well reported in literature [71].

Surface-poisoning of Pt by CO is a common phenomenon in oxidation catalysts and is the reason for the lack of WGS activity at low temperature over Pt. The results above are in line with those of Cant *et al.* who report that NO removal over Pt in the presence of CO and H<sub>2</sub> requires temperatures above 220 °C. In contrast to Pd, Pt un-

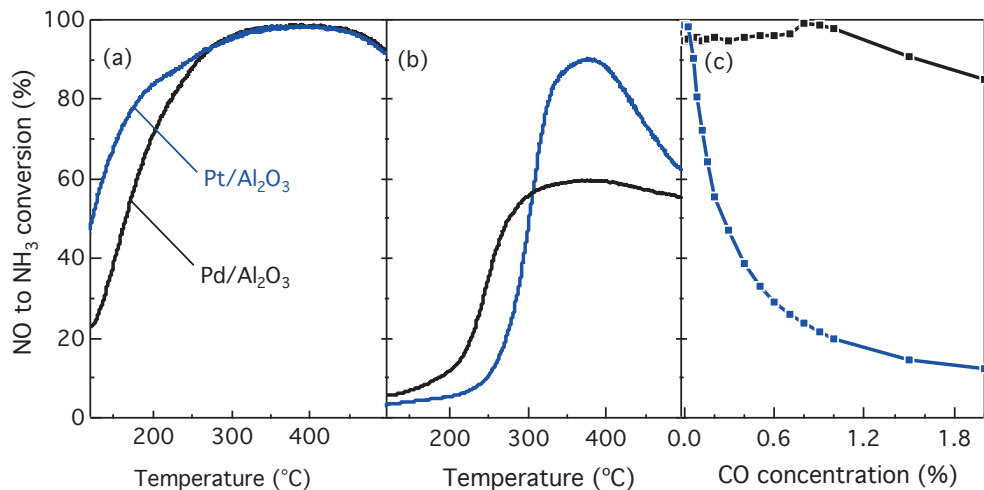


Figure 4.5: Conversion of NO to ammonia over alumina supported Pt and Pd during temperature programmed reaction in the presence of (a) NO + H<sub>2</sub> and (b) NO + CO + H<sub>2</sub>O. Temperature ramp rate of 6 °C/min and balance Ar employed so as to maintain a space velocity of 40 000 h<sup>-1</sup>. (c) Conversion of NO to NH<sub>3</sub> observed at 300 °C over Pd and Pt/Al<sub>2</sub>O<sub>3</sub> as a function of varying CO concentration. A constant flow of NO (500 ppm) + H<sub>2</sub> (1500 ppm) was used whilst varying the CO content between 0 and 2 vol.%. Ar was used as balance and space velocity was maintained at 40 000 h<sup>-1</sup>

dergoes significant coverage by strongly adsorbed CO which displaces NO and hinders the dissociative adsorption of H<sub>2</sub>. Adsorbed H atoms are required for the removal of O adatoms formed via dissociative NO adsorption, but can also aid in the dissociation of NO at low temperature as discussed in section 4.1. The poisoning of Pt by CO was also seen in this work via *in situ* DRIFT spectra taken in the presence of NO, CO, H<sub>2</sub>O and varying oxygen concentrations. As the concentration of oxygen in the supplied feed decreased, the build-up of linearly adsorbed CO on Pt was significantly more pronounced than on Pd. This suggested that oxygen addition may be a sufficient method of alleviating the poisoning effect of CO on Pt active sites when present in very low concentrations. Indeed, this was seen during WGS-assisted oxygen-sweep experiments at 350 °C. A benefit was seen with regards to the activity for ammonia formation when feeds containing low amounts of oxygen ( $S = 0.53$ ) were used in comparison to feeds where oxygen was absent ( $S = 0.33$ ).

The poisoning of Pt by CO at low and intermediate temperature was studied further and is presented in Figure 4.5c [72]. Severe poisoning of Pt active sites by CO is seen at 300 °C, whereas the Pd-containing sample remained largely unaffected. This effect is well reported in literature. Macleod *et al.* have conducted numerous studies on lean NO<sub>x</sub> reduction using H<sub>2</sub> + CO mixtures over both Pt/Al<sub>2</sub>O<sub>3</sub> and Pd/Al<sub>2</sub>O<sub>3</sub> [73, 74] and found that CO addition has very differing effects on Pt and Pd; detrimental in the

case of Pt and beneficial for Pd. The formation and subsequent hydrolysis of CNO is reported to take place over Pd in the presence of NO, CO + H<sub>2</sub> by Voorhoeve *et al.* [75]. Since this species is also able to form on Pt-containing catalysts, it is important to clarify that NCO formation on Pt requires higher temperature than those employed when the detrimental effect of CO was observed. Typically, the onset for formation of CNO on Pd occurs at temperatures about 70 °C lower than that of Pt [73], which correlates with the difference in T<sub>50</sub> values obtained in our work (Figure 4.5 b). An additional observation, made by Almusaiteer *et al.* [76] is that, in the absence of O<sub>2</sub>, H<sub>2</sub> itself acts as a promoter for the reaction of NO with CO on Pd/Al<sub>2</sub>O<sub>3</sub>. They conclude that, when NO and H<sub>2</sub> adsorb dissociatively onto noble-metal active sites, adsorbed H adatoms can react with O and N to form water and ammonia respectively. An increase in CO<sub>2</sub> is also observed when H<sub>2</sub> was present in the feed, due to reaction of adsorbed O with adsorbed CO. The combination of these mechanisms are responsible for the maintained availability of active sites for NO<sub>x</sub> reduction over Pd whilst in the presence of CO.

### Support effects

With regards to the suitability of metal-oxide supports in automotive catalysis, it is generally accepted that materials should have high hydrothermal stability and high surface area. Alumina and silica were chosen as materials of interest, partly due to their high surface area and common usage in TWC formulations. In addition, high

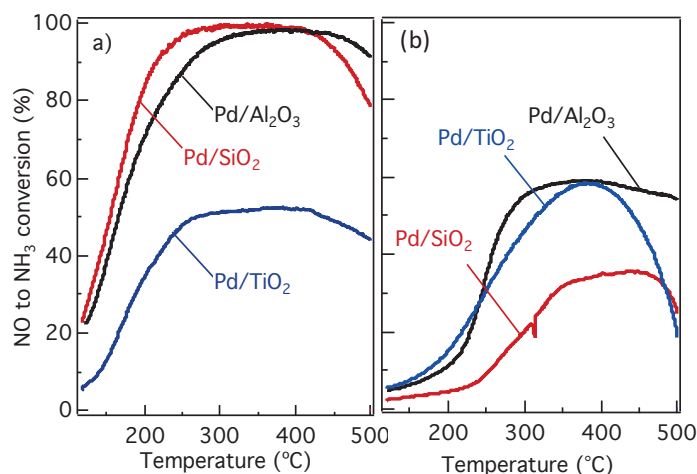


Figure 4.6: Ammonia formation over silica, alumina and titania supported Pd as a function of reactor inlet temperature. The feed consisted of either (a) 500 ppm NO + 1500 ppm H<sub>2</sub> or (b) 500 ppm NO + 1500 ppm CO + 2 vol.% H<sub>2</sub>O. In each case, balance Ar was employed to maintain the space velocity at 40 000 h<sup>-1</sup>.

selectivity to  $\text{NH}_3$  is achieved over these supports during the reaction of  $\text{NO}$  and  $\text{H}_2$ , when used in combination with  $\text{Pt}$  and  $\text{Pd}$ , has been reported by Okumura *et al.* [77]. Titania was also investigated as a material of interest in this work as it has been reported to promote the formation of surface cyanate species in feeds containing  $\text{NO}$  and  $\text{CO}$  [78]. This was seen as beneficial for this work because, as discussed in section 2.3, the hydrolysis of isocyanates is a well-known pathway for ammonia formation from nitric oxide. Furthermore, the authors also suggest that when used as a support, alumina promotes the hydrolysis of surface cyanates to form ammonia [78].

The activity for  $\text{NH}_3$  formation over  $\text{SiO}_2$ ,  $\text{Al}_2\text{O}_3$  and  $\text{TiO}_2$  supported  $\text{Pd}$  is shown in Figure 4.6. The figure illustrates the activities for reaction of  $\text{NO}$  with either a direct supply of  $\text{H}_2$  (panel a) or a mixture of  $\text{CO}$  and  $\text{H}_2\text{O}$  (panel b). In panel (a), low activity (about 50 %) over the titania supported catalyst is observed compared to almost full conversion of  $\text{NO}$  to  $\text{NH}_3$  over the catalysts with alumina and silica as supports. When characterizing the  $\text{Pd}/\text{TiO}_2$  sample, it was found that a significant decrease in specific surface area of the sample from 337 to 42  $\text{m}^2/\text{g}$  as a result of the calcination step in the synthesis procedure. A phase-change from anatase to rutile was originally suspected to be the explanation for this difference. However, XRD analysis confirmed that the  $\text{TiO}_2$  remains in the form of anatase but, as the intensity of the diffraction peaks increases significantly, it can be concluded that the primary particles of the porous titania have grown considerably as a result of calcination. It is possible that the growth of such particles results in the engulfment of  $\text{Pd}$  active sites. As access to these sites is required for  $\text{NO}$  adsorption and dissociation,  $\text{NH}_3$  formation becomes limited over this sample. When this sample was analysed *in situ* using DRIFT spectroscopy, the intensity of the IR bands corresponding to surface bound species was very low. This further suggests that the adsorption capacity for reactant molecules on this sample is limited. Although a lower calcination temperature may have prevented the dramatic loss of surface area during the preparation procedure, this material would be unsuitable for use in automotive applications. This is said because of the high temperatures (up to 850 °C) that the aftertreatment system can be exposed to in gasoline vehicles [12]. Interestingly, when in the presence of WGS-assisted feed gas compositions, the activity of the titania supported sample becomes comparable to that of the alumina supported sample. The combined synergy of these supports, ammonia formation via the enhanced formation and hydrolysis of surface cyanates, is therefore a promising area for future investigation, although the thermal stability of titania would need to be addressed, possibly by the introduction of stabilizers such as zirconia.

The activity for  $\text{NH}_3$  formation of the silica sample is significantly affected in the presence of WGS-assisted conditions. This observation is in line with a study by Grenoble *et al.*, who also report a dramatic decrease in activity over silica supported catalysts compared to alumina supported catalysts when studying the WGS reaction [79]. The difference in activity relates to the activation of the water molecule which takes place on active sites on the support. Supports that readily and reversibly interact with water, such as alumina, exhibit superior activity compared to  $\text{SiO}_2$  which consists only of

tightly bound hydroxyl groups [80].

## Addition of promoters

### *Barium oxide*

Modification of Pd/Al<sub>2</sub>O<sub>3</sub> by baria was investigated in Paper III. The motivation behind the use of this promoter was its role in hybrid lean NO<sub>x</sub> trap (LNT)-SCR systems. This system, as with the passive-SCR system, depends on periodic switching between lean and rich operation. The difference between these systems is that, during lean phases, NO<sub>x</sub> is stored on the LNT catalyst before being reduced to N<sub>2</sub> by hydrocarbons, CO and H<sub>2</sub> during subsequent rich periods. As ammonia can be formed during the rich regeneration phase, according to eqn 17, an SCR catalyst is placed downstream for ammonia storage. The stored ammonia can then be used to react with any slipped NO<sub>x</sub> which is not stored over the LNT during the subsequent lean phase [81, 82, 83].



The observed ammonia formation from stored nitrates on the BaO component of the LNT during rich engine operation was thus thought of as a beneficial reaction that could be exploited in passive-SCR applications.

Baria was impregnated into a pre-synthesized batch of Pd/Al<sub>2</sub>O<sub>3</sub> using a solution of barium nitrate. As the dispersion of Pd throughout the parent Pd/Al<sub>2</sub>O<sub>3</sub> sample was homogeneous, it was assumed that the noble metal particle size distribution in the Ba-modified sample would be comparable. This was assumed because, during synthesis of the parent sample, strong and localized bonds form between Pd and tetrahedral sites of the  $\gamma$ -alumina support [84]. After the sample is stabilized via calcination, it is highly unlikely that the active phase undergoes significant change as a result of the secondary impregnation step, namely the addition of barium. STEM-EDX analysis of the sample (Figure 4.7a) indicated that, in addition to small well-distributed particles of barium, most likely in the form of baria, throughout the alumina support (left-hand panels), there were also large needle-like crystallites which had no interaction with the support (right-hand panels). These needles were attributed to Ba(OH)<sub>2</sub>.H<sub>2</sub>O.

Figure 4.7 b shows the comparative ammonia formation activity of the Pd/Al<sub>2</sub>O<sub>3</sub> reference sample and the barium-modified sample versus reactor inlet temperature. The feed was composed of a mixture of NO and H<sub>2</sub>. The loss of activity over the sample containing barium is most likely explained by two major factors; Firstly, the number of available palladium sites has decreased as a result of the barium impregnation step. As previously discussed, the noble metal phase is generally considered to be the active site for ammonia formation in the NO + H<sub>2</sub> reaction. Indeed, it has been reported

that, when exposed to such strongly reducing conditions, BaO migrates towards and partially encapsulates Pt sites. This coverage is a reversible effect and when conditions become oxidizing, barium will migrate away from the platinum sites [85]. This is an effect of the strong metal-support interaction (SMSI) between noble metal and barium and it is thus likely that the same effect would be seen for palladium [86]. Secondly, charge transfer from barium to palladium affects the electronic properties of the palladium [87, 88], altering the selectivity towards  $\text{NH}_3$ .

The barium-modified sample was also seen to exhibit  $\text{NO}_x$  storage properties during transient cycling between lean and rich conditions when hydrogen was directly available in the feed (Figure 4.7c). When excess oxygen was added to the feed, NO slipped over the sample as previously seen for the unmodified sample. However, instead of an

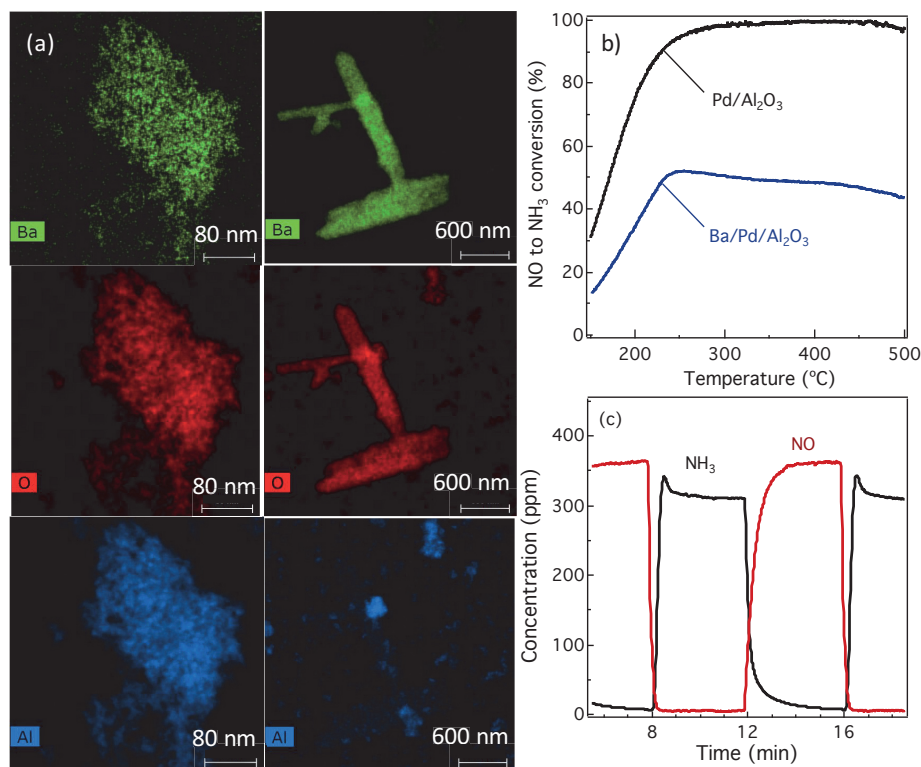


Figure 4.7: (a) STEM-EDX maps of Ba, O and Al for Ba/Pd/ $\text{Al}_2\text{O}_3$ , (b) Ammonia formation from  $\text{NO} + \text{H}_2$  over the reference (black) and Ba-modified sample (blue) as a function of reactor inlet temperature, (c) Transient formation and slip of  $\text{NH}_3$  and NO respectively over the Ba-modified sample versus time of reaction. The feed consisted of a constant stream of  $\text{NO} + \text{H}_2$  into which periodic pulses of excess oxygen was supplied every 4 minutes. The reaction temperature was  $250\text{ }^{\circ}\text{C}$  and balance Ar was employed.

immediate slip of all NO (resulting in very square reaction profiles) some of the NO is instead stored. This is indicated by the slope of the outlet NO concentration, which requires around 200 s for full saturation of the sample by NO. During the storage process, NO is oxidized on palladium sites and subsequently stored in the form of nitrates on the BaO phase. Upon removal of O<sub>2</sub> from the feed, a spike in NH<sub>3</sub> formation is observed before a steady-state response is achieved over the catalyst. This spike occurs due to the release, and subsequent reaction with H<sub>2</sub>, of the stored nitrates according to eqn 17.

### *Cerium oxide*

Ceria impregnation was investigated in this work due to reports of superior WGS reaction (eqn 14) properties throughout literature [89, 90]. Although the majority of studies focus on ceria as a support material, Paper IV showed that the addition of merely 3.6 wt.% cerium into the catalyst formulation results in slight improvement in the WGS-assisted NH<sub>3</sub> formation (Figure 4.8a). As the ceria content of the catalyst is increased, up to a maximum of 38 wt.%, the activity increases significantly further. This effect was seen despite the decrease in specific surface area and palladium dispersion of the samples as a result of increasing ceria content, which would usually lead one to expect a decrease in activity. The high WGS activity observed over ceria is due to the reversible reduction of the oxide via the formation of an oxygen vacancy [91]:



During reaction, CO is able to adsorb onto metal active sites whilst H<sub>2</sub>O dissociation takes place on oxide vacancies present in the ceria [92]. The dissociated H<sub>2</sub>O can then react with adsorbed CO to form CO<sub>2</sub> and the H atoms can either recombine to form the desired H<sub>2</sub> or, if NO is also adsorbed as is the case with the feeds studied in this work, can react stepwise to form the desired ammonia. It was shown that increasing the concentration of ceria within the sample resulted in even higher WGS activity, shifting towards lower light-off temperatures. The higher activity of such samples can be directly correlated to the increased availability of oxide vacancies in the catalyst, leading to an increased probability of H<sub>2</sub>O dissociation.

The ease of reducibility of ceria also results in high oxygen storage capacity (OSC) of the material. The high density of both surface and bulk oxygen vacancies allows the fast exchange of surface oxygen with gas-phase oxygen and enables a high diffusion rate of bulk oxygen towards the catalyst surface [92, 93, 94]. Dynamic OSC is a property which is highly temperature-dependant. At low temperature (< 300 °C) it is generally accepted that only surface and near-surface lattice oxygen is involved in the dynamic OSC of a sample. As temperature increases, oxygen spillover processes are accelerated and a higher contribution of lattice oxygen is available for reaction, resulting in an

increase in dynamic OSC of the material.

In Paper III, a benefit was seen from the OSC properties of the ceria-modified sample, in the form of a temporary formation of ammonia in the presence of globally oxidizing reaction conditions at low temperature (250 °C, Figure 4.8b). In the experimental protocol conducted, the oxygen feed was decreased stepwise in terms of concentration, starting from a large excess of that required for stoichiometric conditions to be met. Thus, when exposed to the first stoichiometric value at which the formation of low amounts of ammonia is observed ( $S = 1.53$ ), this may indicate the concentration at which the ceria is able to buffer the oxygen slightly, extending the period required for total oxidation of the sample to take place. This is suggested because a near but not fully steady-state response regarding the formed  $\text{NH}_3$  is reached over these globally lean points, which may indicate that some active sites of the sample are exposed to a locally reducing environment due to the unique oxygen storage properties of ceria. If these steps however, were allowed to reach steady-state as a result of extended periods of time under oxidizing conditions, the oxygen storage capacity of the ceria will likely diminish and the palladium sites subsequently become oxidized, which may result in a

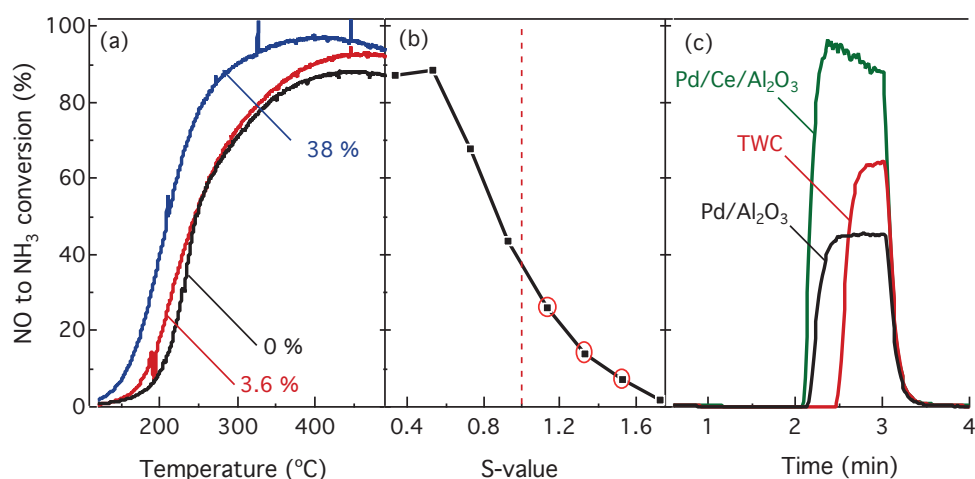


Figure 4.8: (a) NO to  $\text{NH}_3$  conversion over pure  $\text{Pd}/\text{Al}_2\text{O}_3$  and samples modified with 3.6 or 38 wt.% Ce during temperature programmed reaction in the presence of 500 ppm NO, 1500 ppm CO and 2 vol.%  $\text{H}_2\text{O}$ . (b) Steady-state conversion to  $\text{NH}_3$  as a function of the stoichiometric number,  $S$ , of the feed gas at 250 °C over  $\text{Ce}/\text{Pd}/\text{Al}_2\text{O}_3$  in the presence of 500 ppm NO and 1500 ppm  $\text{H}_2$ . The  $\text{O}_2$  concentration was varied corresponding to feed gas compositions of  $S$ -values between 0.33 and 1.73. Circled data points represent responses which have not yet reached steady-state. (c) Transient conversion of NO to  $\text{NH}_3$  at 500 °C over  $\text{Pd}/\text{Al}_2\text{O}_3$ ,  $\text{Pd}/\text{Ce}/\text{Al}_2\text{O}_3$  and the TWC during cycling between rich ( $S = 0.688$ ) and lean ( $S \gg 1$ ) feed compositions for 60 and 120 seconds respectively.

loss of activity for ammonia formation.

Since passive-SCR depends on periodic switching between lean and rich operation, the oxygen storage properties of ceria may be problematic, as oxygen buffering is an undesirable property for this application. That is to say, prior to ammonia formation upon switching from lean to rich engine operation, oxygen must be removed from the catalyst surface so that hydrogen is not consumed by formation of water [26]. The period required for these conditions to be met can result in a delay in the ammonia formation if the OSC of the employed catalyst is high. In Paper V, transient ammonia formation activity of Pd/Ce/Al<sub>2</sub>O<sub>3</sub> was compared to a commercially available TWC in the presence of complex feeds (Figure 4.8c). The TWC washcoat used has an order of magnitude higher dynamic OSC (370  $\mu$ mol) in comparison to the model Pd/Ce/Al<sub>2</sub>O<sub>3</sub> (40  $\mu$ mol). As no NH<sub>3</sub> formation was observed over the TWC during short-length pulses, the experiment was repeated with a longer duration of lean and rich periods whilst maintaining (120 and 60 s respectively). The results are displayed in Figure 4.8 (c). It can be seen that the required time before NH<sub>3</sub> formation is observed over the TWC is approximately 30 s, a period that is substantially longer than its Pd-based counterparts and would result in a significant fuel penalty. Although the inclusion of ceria within the washcoat formulation may be beneficial for the provision of hydrogen for ammonia formation, the combination of ceria with zirconia results in a substantial increase in OSC [95, 94, 96] which may be too high for this application. Traditionally, zirconia is used to thermally stabilise the ceria component of the conventional TWC [97, 98]. Thus, a future area of investigation may therefore be to determine whether ceria can be made more thermally durable without incurring a significant increase in OSC.

When the temperature is low ( $< 200$  °C) and the feed gas compositions are rich, significant activity for N<sub>2</sub>O formation is observed over ceria-containing samples when CO and H<sub>2</sub>O are present in the feed. This activity window shifts towards lower temperature and higher concentrations are formed as the ceria content of the sample is increased. The formation of N<sub>2</sub>O in this temperature regime is most likely related to the limited WGS activity over the samples below 200 °C. When H<sub>2</sub> is not formed over the samples and the extent of dissociative adsorption of NO is limited, it is likely that the recombination of adsorbed NO with N adatoms becomes the preferred reaction.

### 4.3 Catalyst structure-function relationship

*In situ* XAS and DRIFTS studies were performed in Papers VI and VII to study changes in noble-metal oxidation state and surface-species coverage during the formation of ammonia from NO and H<sub>2</sub>. Particular focus was directed towards the effect of oxygen on the reaction because, as previously discussed, ammonia formation is increasingly suppressed as feeds become more oxidizing in nature.

#### *Pt/Al<sub>2</sub>O<sub>3</sub>*

In Paper VI, a model Pt/Al<sub>2</sub>O<sub>3</sub> catalyst was investigated. The Pt L<sub>III</sub> edge was measured at 350 °C in the presence of constant concentrations of NO and H<sub>2</sub> whilst the concentration of O<sub>2</sub> was adjusted to correspond to S-values between 0.33 and 1.53. A sharp absorption at this edge (11,560 eV) was seen over all samples (Figure 4.9 a) which increases in intensity as the oxygen content of the reaction feed increases. The L<sub>III</sub> edge XANES corresponds to excitation of an electron from the 2p<sub>3/2</sub> core states to

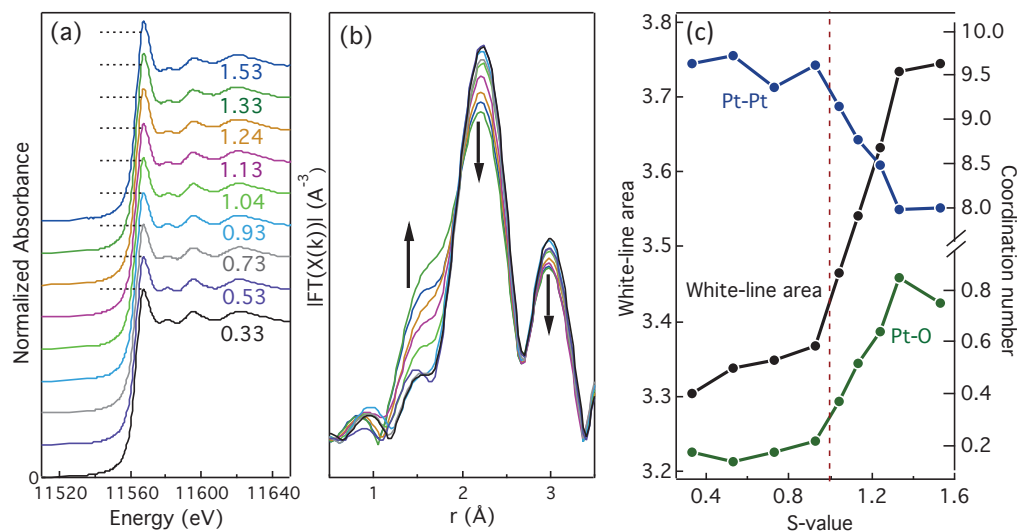


Figure 4.9: *In situ* spectroscopic data obtained during exposure of Pt/Al<sub>2</sub>O<sub>3</sub> to NO and H<sub>2</sub> whilst varying the S-value of the feed (displayed on spectra) (a) X-ray absorption spectra of the Pt L<sub>III</sub> edge at 11,560 eV. The dotted line indicates the relative height of the white-line of the reduced sample (S = 0.33). (b) Fourier transformed EXAFS spectra showing the Pt-O component at 1.5 Å and the Pt-Pt component at 2.2 and 3.0 Å. (c) evolution of white-line area of the XANES spectra as well as Pt-Pt and Pt-O coordination number obtained from fitting of EXAFS data at corresponding S-values of feed.

$5d_{3/2}$  and  $5d_{5/2}$  states [99]. The absorption intensity of the white-line is proportional to 5d-electron vacancies in the Pt. A large white-line is observed for oxidized Pt, whereas a small white-line is observed when Pt is in a reduced state [100]. Thus, the increasing absorbance represents an increase in oxidation state of the Pt as the feed becomes increasingly oxidizing. The corresponding EXAFS spectra are displayed in Figure 4.9b. The arrows indicate the direction of growth/decrease of the peaks as the stoichiometric value of the reaction feed increases. The growth in the Pt-O components of the sample (1.5 Å), accompanied by a decreasing contribution from Pt-Pt components (2.2 and 3.0 Å), confirm that a physical change of the Pt phase within the sample occurs as a result of increasing the O<sub>2</sub> concentration of the feed. The change in white-line area and co-ordination number of Pt-Pt and Pt-O components as a function of the S-value is displayed in Figure 4.9c. Although a small increase in white-line area is observed upon increasing the S-value of the feed whilst remaining in the net-reducing regime, no significant change in Pt-O component of the EXAFS region is seen. This is indicative of an adsorbed surface layer of oxygen atoms rather than the formation of platinum oxides. As discussed in section 4.1, when  $S < 1$  it is likely that the majority of fed O<sub>2</sub> is reduced by H<sub>2</sub> to form H<sub>2</sub>O. However, when  $S > 1$  the O<sub>2</sub> concentration exceeds that required for total oxidation of the fed H<sub>2</sub> and the formation of Pt oxides occurs rapidly. This trend is seen in both the white-line area and EXAFS region, proving that a structural change of the sample occurs.

It is apparent that an inverse relationship between platinum oxide formation and NH<sub>3</sub> generation exists, suggesting that for platinum-based samples to be active, the noble metal must be present in the reduced form. It is well known that the adsorption of NO and O<sub>2</sub> on noble metal active sites is a competitive process [101, 102]. As temperature increases, the adsorption of O<sub>2</sub> is preferred due to its rapid dissociation, whereas the rate of NO desorption from the catalyst is considerable [103]. Indeed, our results show that the adsorption of oxygen is preferred even at the intermediate temperature of 350 °C. They also show that the presence of excess oxygen facilitates the formation of platinum oxides. The rapid rate of desorption of NO from the catalyst surface at this temperature results in a decreased probability of interaction, and thus reaction, with other surface species leading to high reactor outlet concentration of NO, as seen in figure 4.3a. Furthermore, as the dissociative adsorption of NO is preferred over reduced platinum sites [104], it was suspected that oxide formation limits the extent of NO dissociation due to weak interaction with the platinum oxide.

In order to confirm this statement, first-principle calculations using density functional theory (DFT) were utilized and it was found that as the oxidation of Pt increases, the overall interaction with NO decreases. In figure 4.10a the energy of adsorbed and dissociated NO on Pt (111) is shown together with the activation energy of the transition state for oxygen coverages ranging from 0 (clean surface) to 4/9 monolayers. The structures of the initial, transition and final state are shown in figure 4.10b. As the oxygen coverage increases, destabilization of adsorbed NO occurs, accompanied by increasing activation energy of the transition state. Dissociated NO also becomes

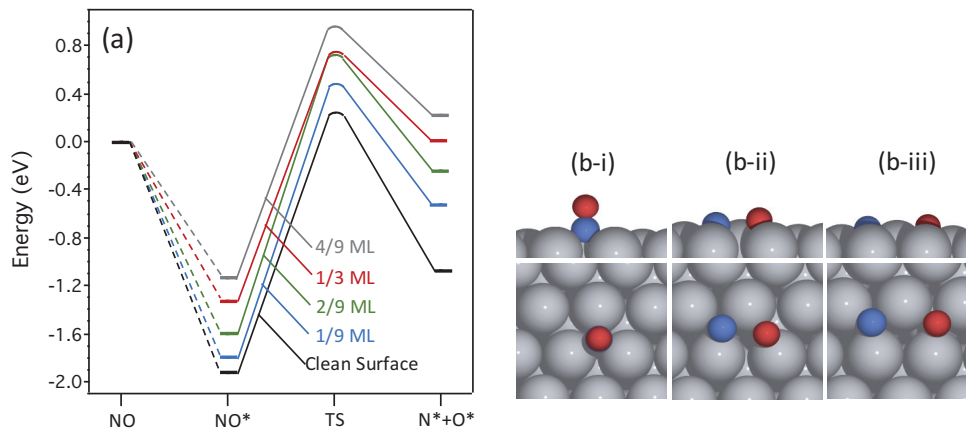


Figure 4.10: (a) Energy profile of NO adsorption and dissociation of NO on Pt (111) as the coverage of oxygen increases from 0 up to 4/9 monolayers (indicated in the figure). (b) The initial (i), transition state (ii) and final (iii) structure are shown in side (upper panels) and top view (lower panels) for NO dissociation on a clean Pt (111) surface.

increasingly destabilized and is energetically unfavourable at a monolayer coverage of 1/3. For the ammonia formation reaction to take place, surface adsorbed N atoms are required for reaction with  $H_2$ . Thus, at a coverage of 1/3 monolayer, the reaction would be effectively hindered. When first-principles calculations were carried out for the surface oxide, no interaction for adsorbed NO was seen and dissociated NO was highly unstable, resulting in spontaneous formation of NO using surface oxygen if necessary.

The dissociation of NO is a prerequisite step, necessary for the subsequent formation of ammonia from adsorbed N and H atoms. Thus, this step was identified as rate limiting with regards to the ammonia formation from feeds containing NO and  $H_2$  in the presence of net-oxidizing conditions.

### *Pd/Ce/Al<sub>2</sub>O<sub>3</sub>*

The change in oxidation state of the Pd phase in a model Pd/Ce/Al<sub>2</sub>O<sub>3</sub> catalyst during ammonia formation from nitrogen oxide was investigated in Paper VII. Two reactions were performed. The first involved feeding a constant stream of NO through the reaction cell together with periodic pulses of H<sub>2</sub>. For the second reaction, NO and H<sub>2</sub> were fed in combination with periodic pulses of O<sub>2</sub> to simulate cycling between lean and rich conditions as would be encountered onboard passive-SCR applications.

When only NO was flowed over the catalyst, a gradual increase in the white-line intensity (WLI) of the Pd K-edge was observed. This effect is seen in the white panels of figure 4.11a and indicates an increase in PdO components of the sample. The increase in PdO is reflective of the oxidizing nature of NO. As the reaction is performed at 350 °C, NO adsorbs dissociatively on Pd and the accumulation of adsorbed O atoms leads to the formation of PdO [105]. The steady-state *in situ* DRIFT spectrum acquired for NO adsorption over Pd/Ce/Al<sub>2</sub>O<sub>3</sub> supports this hypothesis due to the presence of the peak representative of linearly adsorbed NO on Pd<sup>+</sup> (1775 cm<sup>-1</sup>). As the sample is pre-reduced by flowing H<sub>2</sub> prior to reaction, the presence of this peak signifies oxidation of the metallic Pd<sup>0</sup> species to Pd<sup>+</sup> as a result of NO adsorption. The dissociative

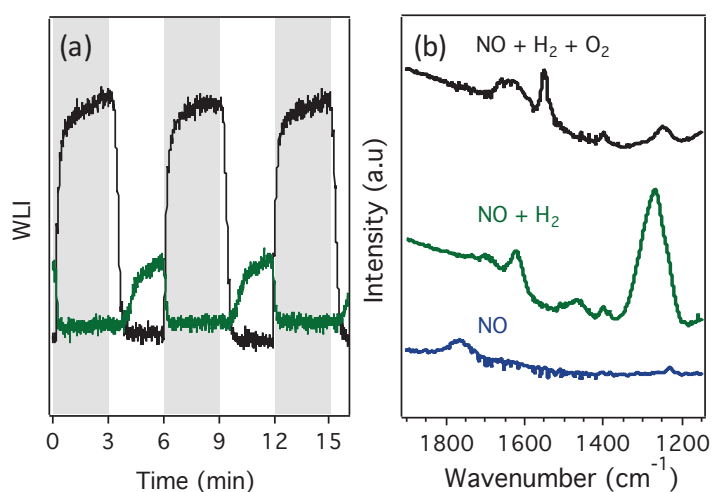


Figure 4.11: (a) The change in white-line intensity of the Pd/Ce/Al<sub>2</sub>O<sub>3</sub> sample as a result of either H<sub>2</sub> pulses into a constant supply of NO (green) or O<sub>2</sub> pulses into a constant feed of NO + H<sub>2</sub> (black). Grey panels indicate the period of injection of H<sub>2</sub> or O<sub>2</sub>. Reaction temperature 350 °C. Ar balance used to maintain a flowrate of 75 ml/min. (b) Steady-state *in situ* DRIFT spectra taken when the catalyst is exposed at 350 °C to NO only (blue), a mixture of NO + H<sub>2</sub> (green) or a combination of NO, H<sub>2</sub> + O<sub>2</sub> (black).

adsorption of NO on the sample is seen by the small peak representative of surface nitrates ( $1235\text{ cm}^{-1}$ ) which occurs via the reaction of adsorbed NO with O adatoms. Upon introduction of  $\text{H}_2$  to the feed, the WLI of the sample rapidly decreases, indicating a transition from oxidized to reduced Pd. The slow oxidation and fast reduction of Pd suggests a hysteresis in the oxidation-reduction behaviour of the Pd particles. Assuming that only chemisorbed species exist on the Pd surface, the hysteresis is a result of the difference in the dissociative adsorption kinetics of NO and  $\text{H}_2$ . In this case, NO dissociation is relatively slow compared to  $\text{H}_2$  dissociation. However, if a surface oxide is formed on the Pd the hysteresis behaviour is further complicated by the difference in kinetics for oxide formation and removal.

When excess  $\text{O}_2$  is pulsed over the sample whilst flowing NO and  $\text{H}_2$ , the WLI of the sample increases much more rapidly and to a higher extent than the change in WLI observed as a result of exposure to NO alone. The increased intensity of the white-line in the presence of  $\text{O}_2$  indicates a deeper oxidation of the Pd particles. During pulses of  $\text{O}_2$  excess the majority of fed NO slips through the cell unreacted, as was seen during the experiments over Pt/ $\text{Al}_2\text{O}_3$  discussed earlier in this section. It is therefore assumed that NO dissociation also occurs preferentially over reduced Pd sites. Indeed, even the low degree of Pd oxidation by NO itself limits the dissociative adsorption of NO. This was seen by the increasing NO slip which coincided with the growth of PdO components of the sample. The steady-state *in situ* DRIFT spectrum acquired in excess  $\text{O}_2$  showed the presence of surface nitrate peaks on the sample ( $1560$ ,  $1403$  and  $1235\text{ cm}^{-1}$ ). This indicates that, although dissociation is limited on the sample, NO adsorption still occurs although its extent may be minor.

## Concluding remarks

This work targets the formation of ammonia from nitrogen oxide over supported noble metal catalysts. The thesis objective was to deepen the understanding of how ammonia formation is achieved, and limited, by feed mixtures containing NO and other reactants. The effect on activity by components commonly found in three-way catalysts was also investigated. In order to achieve this, a bottom-up research approach was used with regards to the complexity of the reactions and catalyst formulations investigated.

Addressing the catalyst formulation, we have identified Pd/Ce/Al<sub>2</sub>O<sub>3</sub> as a promising material. This sample exhibited high activity for ammonia formation in the presence of model feed gas mixtures using (i) a direct source of hydrogen and (ii) hydrogen formed via the water-gas-shift reaction. As water is available in abundance onboard automobiles, the enhanced activity over ceria-impregnated samples may be beneficial for application. Pd/Ce/Al<sub>2</sub>O<sub>3</sub> also showed high activity for ammonia formation in the presence of complex feed gas compositions more representative of what may be encountered in the exhaust of a lean-burn gasoline vehicle. This sample exhibited higher activity for ammonia formation than the three-way catalyst tested in this study. As the current agreement in the literature is that employing three-way catalysts is sufficient for ammonia formation, this work highlights that there is work to be done with regards to modifying the formulation for suitability in passive-SCR systems. For example, whilst we show that an increase in oxygen storage capacity is favourable for the provision of hydrogen, it was also seen that, when the oxygen storage of the sample is too high, a significant delay in ammonia formation occurs upon switching to rich operation. This delay is particularly prominent over the three-way catalyst investigated, due to excessive oxygen storage as a result of the combination of ceria with zirconia. This combination is used in three-way catalysts today to ensure thermal stability of the ceria, but also because high oxygen storage capacity allows the three-way catalyst to continue working under stoichiometric conditions despite fluctuations in air-to-fuel ratio. As excessive oxygen storage capacity renders the three-way catalyst unsuitable for passive-SCR application, a future area of interest is the thermal stabilisation of ceria by using compounds which do not alter the storage capacity of the catalyst.

The suppression of ammonia formation as feeds tend towards stoichiometric and globally oxidizing conditions is of particular concern for passive-SCR application. A considerable fuel penalty will be experienced if long periods of rich operation are necessary to fully saturate the SCR catalyst with ammonia. It would therefore be beneficial if significant and instantaneous activity could be achieved at near-stoichiometric operation. The effect of oxygen on the chemistry of ammonia formation in model feed gas compositions has been of particular focus in this work. *In situ* X-ray absorption spectroscopy and DFT analysis were used to explain the NO slip observed over Pt/Al<sub>2</sub>O<sub>3</sub> when net-oxidizing conditions are present, as reported in Paper II. In addition to the oxidation of the H<sub>2</sub> reductant to form H<sub>2</sub>O, a rapid growth in Pt-oxides was seen in the sample when oxidizing feeds were examined. This was explained by weak interaction with the noble metal phase of the sample as it became increasingly oxidized. When fully oxidized, the DFT calculations predicted no interaction for adsorbed NO. As NO dissociation is a prerequisite step for NH<sub>3</sub> formation via sequential surface reactions between adsorbed N and H atoms, we propose this as the rate-limiting step for NH<sub>3</sub> formation from NO and H<sub>2</sub> in the presence of oxidizing conditions.

In future work, low-temperature NO<sub>x</sub> reduction is an interesting area for potential investigation. Ammonia formation activity was low below 200 °C over the materials investigated in this work. In the first minutes of engine operation, so-called cold starts, the temperature of the catalytic converter is too low to operate efficiently, leading to increased NO<sub>x</sub> emissions from the vehicle. This is increasingly a problem with the development of modern engines and the use of start-stop technology which results in cold exhausts. Ideally, if NH<sub>3</sub> formation could be achieved over the AFC at low temperature (< 200 °C), this would benefit the passive-SCR concept as the NH<sub>3</sub> storage capacity of SCR catalysts is considerable at low temperature. This calls for the production of novel materials, perhaps not common in TWC formulations, that are active in the low-temperature region.

Furthermore, as hydrogen formation is viable from sources of hydrocarbon via steam reforming, the use of renewable fuels, i.e. alcohols, is also an interesting research area for passive-SCR applications.

## Acknowledgements

This work was performed in collaboration with Volvo Car Corporation AB, Haldor Topsøe A/S and the Combustion Engine Research Centre at Chalmers University of Technology within the framework of the Swedish Energy Agency FFI program (project numbers P35561-1 and P35561-2). The work has mainly been performed within the Competence Centre for Catalysis (KCK), which is hosted by Chalmers University of Technology. Financial support was provided by the Swedish Energy Agency and KCK member companies; AB Volvo, ECAPS AB, Haldor Topsøe A/S, Volvo Car Corporation AB, Scania CV AB and Wärtsilä Finland Oy.

Parts of the work have also been performed at synchrotron research facilities ESRF and Max IV Laboratory. The provision of beamtime is gratefully acknowledged.

I would also like to thank:

My wonderful family, who always support my decisions no matter how crazy they may seem. For embracing and encouraging my nerdy side from the day I started school. And for always being there for me when I need you. There is no way I could have come this far without you, I love you all.

Freddy, the sweetest, most supportive fiancée I could ever have hoped for. Your belief in me knows no bounds and gives me such confidence in what I can achieve. I can't wait for whatever our next adventures together may bring!

My main supervisor, Associate Professor Per-Anders Carlsson, and examiner, Professor Magnus Skoglundh. Thank you both for giving me the freedom and trust to drive this project in the direction it took. For always having an open door and being there to motivate and support me during the more challenging moments of this project.

All of the colleagues (past and present) at KCK and TYK for creating such a positive working environment. I have made some truly wonderful friends, friendships that I hope will last a lifetime.

David Anderson and Colin Murphy, my chief editors! Thank you so much for the time you have spent reading this thesis and for making me aware of my backwards sentences and very British approach to making statements ;) I really appreciate all of your help.

All of the people I have had the pleasure of collaborating with over the years and those I have met at conferences along the way that have been so encouraging.

Finally (and I can't thank them enough!) Ulf Stenman, Lennart Norberg and Lasse Urholm, for their support in the lab. Ulf, I thank you for always being available (no matter what time it is) and for always leaving me with 'jingle bells' stuck in my head no matter what time of year it is. Lennart and Lasse, the positive influence you've had in the labs during the short time you've been here is phenomenal.

## Bibliography

- [1] J A Anderson and M Fernández García. *Supported Metals in Catalysis*. Imperial College Press, 2012.
- [2] K Skalska, J S Miller, and S Ledakowicz. *Sci. Total Environ.*, 408:3976–3989, 2010.
- [3] Number of vehicle in use worldwide. <http://www.statista.com/statistics/281134/number-of-vehicles-in-use-worldwide>.
- [4] M A Gómez-García, V Pitchon, and A Kiennemann. *Environ. Int.*, 31:445–467, 2005.
- [5] H Bosch and F Janssen. *Catal. Today*, 2:369–379, 1988.
- [6] Emission Standards European Union. <https://www.dieselnet.com/standards/eu/ld.php>.
- [7] A Fritz and V Pitchon. *Appl. Catal. B: Environ.*, 13:1–25, 1997.
- [8] M Chiron. *Stud. Surf. Sci. Catal*, 30:1–10, 1987.
- [9] Y Ji, J-S Choi, M Crocker, and M Naseri. *Catal. Today*, 136:146–155, 2008.
- [10] Y Liu, M P Harold, and D Luss. *Appl. Catal. B: Environ.*, 121:239–251, 2012.
- [11] S M Park, M-Y Kim, H-S Han, and G Seo. *Appl. Catal. A: Gen.*, 395:120–128, 2011.
- [12] J Kašpar, P Fornasiero, and N Hickey. *Catal. Today*, 77:419–449, 2003.
- [13] M P Harold. *Curr. Opin. Chem. Eng.*, 1:303–311, 2012.
- [14] G Liu and P-X Gao. *Catal. Sci. Technol.*, 1:552–568, 2011.

- [15] V Y Prikhodko, J E Parks, J A Pihl, and T J Toops. *SAE Int. J. Engines*, 7:1235–1243, 2014.
- [16] P Forzatti, L Lietti, I Nova, and E Tronconi. *Catal. Today*, 151:202–211, 2010.
- [17] C Ciardelli, I Nova, E Tronconi, D Chatterdee, T Burkhardt, and M Weibel. *Chem. Eng. Sci.*, 62:5001–5006, 2007.
- [18] R K Bhattacharyya. *Int. J. Energy Res.*, 23:351, 1999.
- [19] M Koebel, M Elsener, and M Kleeman. *Catal. Today*, 56:335–345, 2000.
- [20] H L Fang and H F M DaCosta. *Appl. Catal. B: Environ.*, 46:14–34, 2003.
- [21] T Johannessen, H Schmidt, J Svagin, J Johansen, J Oeschle, and R Bradley. *SAE Int.*, 2008-01-1027:doi: 10.4271/2008-01-1027, 2008.
- [22] G Fulks, G B Fisher, K Rahmoeller, M-C Wu, E D’herde, and J Tan. *SAE Int.*, 2009-01-0907:doi: 10.4271/2009-01-0907, 2009.
- [23] C Kim, K Perry, M Viola, W Li, and K Narayanaswamy. *SAE Int.*, 2011-01-0306:doi: 10.4271/2011-01-0306, 2011.
- [24] V Y Prikhodko, J E Parks, J A Pihl, and T J Toops. *Catal. Today*, 267:202–209, 2016.
- [25] C D DiGuilio, J A Pihl, J E Parks, M D Amiridis, and T J Toops. *Catal. Today*, 237:33–45, 2014.
- [26] J R Theis, J Kim, and G Cavataio. *SAE Int. J. Fuels Lubr.*, 8:460–473, 2015.
- [27] A J Kean, D Littlejohn, G A Ban-Weiss, R A Harley, T W Kirchstetter, and M M Lunden. *Atmos. Environ.*, 43:1565–1570, 2009.
- [28] I Chorkendorff and J W Niemantsverdriet. *Concepts of Modern Catalysis and Kinetics*. Wiley-VCH, Weinheim, Germany, 2007.
- [29] J R H Ross. *Heterogeneous catalysis: Fundamentals and applications*. Elsevier, Amsterdam, Netherlands, 2012.
- [30] J K Norskov, F Studt, F Abild-Pederson, and T Bligaard. *Fundamental concepts in heterogeneous catalysis*. John Wiley & Sons, Inc., New Jersey, USA, 2015.
- [31] M Lancaster. *Green chemistry: an introductory text*. RSC, Cambridge, United Kingdom, 2010.
- [32] M Bowker. *The basis and applications of heterogeneous catalysis*. Oxford University Press, Inc, New York, USA, 1998.
- [33] O Guralp, G Qi, W Li, and P Najt. *SAE Technical Paper*, 2011-01-0307, 2011.

- [34] K Narayanaswamy, P Najt, W Li, K L Perry, and C H Kim. *Proc. IMechE*, 225:1365–1376, 2011.
- [35] W Li, K L Perry, K Narayanaswamy, C H Kim, and P Najt. *SAE Int. J. Fuels Lubr.*, 3:99–106, 2010.
- [36] M Shelef and R W McCabe. *Catal. Today*, 62:35–50, 2000.
- [37] R J Farrauto and R M Heck. *Catal. Today*, 55:179–187, 2000.
- [38] G C Kolstakis and A M Stamatelos. *Prog. Energy Combust. Sci.*, 23:1–39, 1997.
- [39] J T Kummer. *Prog. Energy Combust. Sci.*, 6:177–199, 1980.
- [40] H Liu. *Chin. J. Catal.*, 35:1619–1640, 2014.
- [41] H-P Jia and E A Quadrelli. *Chem. Soc. Rev.*, 43:547–564, 2014.
- [42] J A Pool, E Lobkovsky, and P J Chirik. *Nature*, 427:527–530, 2004.
- [43] T Shima, S Hu, G Luo, X Kang, Y Luo, and X Hou. *Science*, 340:1549–1552, 2013.
- [44] N V Heeb, A-M Forss, S Brühlmann, R Lüscher, C J Saxer, and P Hug. *Atm. Environ.*, 40:5986–5997, 2006.
- [45] T D Durbin, J T Pisano, T Younglove, C G Sauer, S H Rhee, T Huai, J W Miller, G I MacKay, A M Hochhauser, M C Ingham, R A Gorse, L K Beard, D DiCicco, N Thompson, R J Stradling, J A Rutherford, and J P Uihlein. *Atmos. Environ.*, 38:2699–2708, 2004.
- [46] M Shelef and H S Gandhi. *Ind. Eng. Chem. Prod. Res. Develop.*, 11:393–396, 1972.
- [47] H G Stenger and J S Hepburn. *Energy & Fuels*, 1:412–416, 1987.
- [48] T P Kobylinski and B W Taylor. *J. Catal.*, 33:376–384, 1974.
- [49] M L Unland. *Science*, 179:567–569, 1973.
- [50] M L Unland. *J. Catal.*, 31:459–465, 1973.
- [51] F Solymosi, J Sarkany, and A Schauer. *J. Catal.*, 46:297–307, 1977.
- [52] P R Dasari, R Muncrief, and M P Harold. *Catal. Today*, 184:43–53, 2012.
- [53] L D’Souza, S Barnes, and J R Regalbuto. *Catalysts*, 5:72–, 2016.
- [54] R K Iler. *The chemistry of silica: solubility, polymerization, colloid and surface properties*. John Wiley & Sons, Inc., New Jersey, USA, 1979.

- [55] D W Johnson, P K Gallagher, F J Schnettler, and E M Vogel. *Am. Ceram. Soc. Bull.*, 56:785, 1977.
- [56] S Brunauer, P H Emmett, and E Teller. *J. Am. Chem. Soc.*, 60:309–319, 1938.
- [57] B Sivasankar. *Engineering Chemistry*. Tate McGraw-Hill Publishing Company Ltd., New Delhi, India, 2008.
- [58] M Thommes, K Kaneko, A Neimark, J P Olivier, F Rodriguez-Reinoso, J Rouquerol, and K S W Sing. *Pure Appl. Chem.*, 87:1051–1069, 2015.
- [59] T Takeguchi, S Manabe, R Kikuchi, K Eguchi, T Kanazawa, S Matsumoto, and W Ueda. *Appl. Catal. A: Gen.*, 293:91–96, 2005.
- [60] P Canton, G Fagherazzi, M Battagliarlin, F Menegazzo, F Pinna, and N Pernicone. *Langmuir*, 18:6530–6535, 2002.
- [61] D Kealey and P J Haines. *Analytical Chemistry*. BIOS Scientific Publishers Ltd., Oxford, United Kingdom, 2002.
- [62] C Wang-Hansen, C J Kamp, M Skoglundh, B Andersson, and P-A Carlsson. *J. Phys. Chem. C*, 115:16098–16108, 2011.
- [63] J A Rodriguez, J C Hanson, and P J Chupas. *In-situ characterization of heterogeneous catalysis*. John Wiley & Sons, Inc., New Jersey, USA, 2013.
- [64] J W Niemantsverdriet. *Spectroscopy in Catalysis; an introduction*. Wiley-VCH, Weinheim, Germany, 2000.
- [65] J Yano and V K Yachandra. *Photosynthesis Research*. Springer Science, Dordrecht, Netherlands, 2009.
- [66] C A de Wolf and B E Nieuwenhuys. *Surf. Sci.*, 469:196–203, 2000.
- [67] L-Y Huai, C-Z He, H Wang, H Wen, W-C Yi, and J-Y Liu. *J. Catal.*, 322:73–83, 2015.
- [68] C A Farberow, J A Dumesic, and M Mavrikakis. *ACS Catal.*, 4:3307–3319, 2014.
- [69] J C Summers and K Baron. *J. Catal.*, 57:380–389, 1979.
- [70] S K Matam, E V Kondratenko, M H Aguirre, P Hug, D Rentsch, A Winkler, A Weidenkaff, and D Ferri. *Appl. Catal. B: Environ.*, 129:214–224, 2013.
- [71] N W Cant, D C Chambers, and I O Y Liu. *Appl. Catal. B: Environ.*, 46:551–559, 2003.
- [72] G Doornbos, E Adams, P-A Carlsson, P Gabrielsson, M Folic, I Denbratt, and M Skoglundh. *SAE Technical Paper*, 2015-24-2504, 2015.

- [73] N Macleod and R M Lambert. *Appl. Catal. B: Environ.*, 35:269–279, 2002.
- [74] N. Macleod and R.M. Lambert. *Applied Catalysis B: Environmental*, 46:483–495, 2003.
- [75] R J H Voorhoeve and L E Trimble. *J. Catal.*, 54:269–280, 1978.
- [76] K Almusaiter and S S C Chuang. *J. Catal.*, 180:161–170, 1998.
- [77] K Okumura, T Motohiro, Y Sakamoto, and H Shinjoh. *Surf. Sci.*, 603:2544–2550, 2009.
- [78] N. Macleod, R Cropley, J M Keel, and R M Lambert. *J. Catal.*, 221:20–31, 2004.
- [79] D C Grenoble and M M Estadt. *J. Catal.*, 67:90–102, 1981.
- [80] D C Grenoble. *J. Catal.*, 51:212–220, 1978.
- [81] L Xu and R W McCabe. *Catal. Today*, 184:83–94, 2012.
- [82] V Easterling, Y Ji, M Crocker, M Dearth, and R W McCabe. *Appl. Catal. B: Environ.*, 123-124:339–350, 2012.
- [83] L Castoldi, R Bonzi, L Lietti, P Forzatti, S Morandi, G Ghiotti, and S Dzwigaj. *J. Catal.*, 282:128–144, 2011.
- [84] Márquez. *Appl. Surf. Sci.*, 238:82–85, 2004.
- [85] V Labalme, N Benhamou, N Guilhaume, E Garbowski, and M Primet. *Appl. Catal. A: Gen*, 133:351–366, 1995.
- [86] X Wang, D H Kim, J H Kwak, C Wang, J Szanji, and C H F Peden. *Catal. Today*, 175:78–82, 2011.
- [87] D T Wickham, B W Logsdon, and S W Cowley. *J. Catal.*, 128:198–209, 1991.
- [88] F Klingstedt, H Karhu, A Kalantar Neyestanaki, L-E Lindors, T Salmi, and J Vayrynen. *J. Catal.*, 206:248–262, 2002.
- [89] T Bunluesin, R J Gorte, and G W Graham. *Appl. Catal. B: Environ.*, 15:107–114, 1998.
- [90] Y Li, Q Fu, and Flytzani-Stephanopoulos. *Appl. Catal. B: Environ.*, 27:179–191, 2000.
- [91] B Perada-Ayo, U De La Torre, J R González-Marcos, and González-Velasco. *Catal. Today*, 241:133–142, 2015.
- [92] V M Shinde and G Madras. *Appl. Catal. B: Environ.*, 123:367–378, 2012.

- [93] C Larese, M L Granados, R Mariscal, J L G Fierro, P S Lambrou, and A M Efstathiou. *Appl. Catal. B: Environ.*, 59:13–25, 2005.
- [94] Z Q Han, J Q Wang, H J Yan, M Q Shen, W L Wang, M Wang, and M Yang. *Catal. Today*, 158:481–489, 2010.
- [95] M H Yao, R J Baird, F W Kunz, and T E Hoost. *J. Catal.*, 166:67–74, 1997.
- [96] H S Gandhi, G W Graham, and R W McCabe. *J. Catal.*, 216:433–442, 2003.
- [97] B Yue, R Zhou, X Zheng, and W Lu. *Mater. Chem. Phys.*, 114:722–727, 2009.
- [98] M Pijolat, M Prin, M Soustelle, and P Touret, O an Nortier. *J. Chem. Soc. Faraday trans.*, 91:3941–3948, 1995.
- [99] A N Mansour, J W Cook, and D E Sayers. *J. Phys. Chem.*, 88:2330–2334, 1984.
- [100] Y Nagai, T Hirabayashi, K Dohmae, N Tagaki, T Minami, H Shinjoh, and S Matsumoto. *J. Catal.*, 242:103–109, 2006.
- [101] R Burch, P J Millington, and A P Walker. *Appl. Catal. B: Environ.*, 4:65–94, 1994.
- [102] R Burch and P J Millington. *Catal. Today*, 26:185–206, 1995.
- [103] G F Froment and K C Waugh. *Reaction Kinetics and the Development of Catalytic Processes*. Elsevier, 1999.
- [104] A Martinez-Arias, M Fernandez-Garcia, A Iglesias-Juez, A Hungria, J Anderson, J C Conesa, and J Soria. *Appl. Catal. B*, 31:51–60, 2001.
- [105] A S Mamede, A Leclercq, E Payen, P Granger, and J Grimblot. *J. Mol. Struct.*, 651:353–364, 2003.